Oral *Porphyromonas gingivalis* Infection Induces Epigenetic Changes that Promote Persistence of Cardiovascular Disease Risk

by

Konrad Lehmann

A thesis submitted in partial fulfillment of the requirements for the degree of

Master of Science

Medical Sciences – Oral Biology
University of Alberta

Abstract

In the last two decades, periodontitis has become recognized as a risk factor for cardiovascular disease (CVD), a term that encompasses many circulatory disorders, often underpinned by atherosclerosis. One of the major questions regarding this association has been whether elimination of periodontitis promotes reversal of CVD risk. Studies in edentulous populations have shown that residual CVD risk persists, even with clinically acceptable elimination of periodontitis. Owing to the strong inflammatory components of both diseases, our lab hypothesizes that persistence of CVD risk is in part a function of epigenetic reprogramming of hematopoietic stem cells in the bone marrow during periodontitis, promoting a pro-atherogenic phenotype in the immune system long-term.

To simulate persistence of CVD risk, a bone marrow transplant approach was used. Bone marrow was transplanted into healthy, irradiated pro-atherogenic mice from two syngeneic donor cohorts: mice orally infected with *Porphyromonas gingivalis* (*Pg*) or sham infected. In previous experiments using this transplant approach, mice receiving BM from *Pg*-infected donors displayed increased atherosclerotic lesion burden, providing a strong underpinning to performing epigenetic analysis. Using whole genome bisulfite sequencing of donor bone marrow progenitor DNA, with cross-referencing of transcriptome analysis from recipient bone marrow-derived macrophages, differentially methylated and expressed genes were identified. Systemic lipid phenotype analyses were also performed as initial studies into differences in phenotype between transplant recipient groups.

Mice receiving bone marrow from *Pg*-infected donors displayed a number of notable differences in plasma lipid profiles. These include increased total triglycerides, esterified

cholesterol, very low-density density lipoprotein (VLDL) triglycerides, and decreased high density lipoprotein cholesterol. Transcriptome analysis showed differential expression in oxidative mitochondrial metabolism and cell stress management. When cross-referenced to whole genome bisulfite sequencing data from progenitors, nine genes differentially methylated and expressed were identified as candidate genes for future phenotypic studies. *PON2, APOE, CBR2, NPC2, ATP5O, ATPF1* were found to be hypermethylated and downregulated, while *SLC23A2, ACC1,* and *SORL1* were found to be hypomethylated and upregulated. Based on their epigenetic and expression profiles, enrichment of these genes suggests a pro-oxidative phenotype, contributing to increased cellular oxidized LDL, in addition to increased triglyceride and cholesterol accumulation. Impaired cholesterol trafficking, as well as catabolism of triglyceride rich lipoproteins may explain the VLDL/triglyceride/esterified cholesterol phenotype data.

Presently, our experiments have suggested that macrophages originating from the bone marrow of mice infected by *Pg* exhibit a more pro-atherogenic phenotype, which may be guided by changes in DNA methylation in upstream progenitors during hematopoiesis. If our hypothesis is supported by future experiments, this will necessitate the development of CVD therapeutics targeting epigenetic processes. Our findings may have broader applicability to other CVD risk factors which are also known to leave increased risk after removal, such as diabetes and smoking.

Preface

In Chapter 3, sections 3.1-3.4, and corresponding figures 1-4 are part of unpublished data from work done by Dr. Mohamed Omar, a PhD candidate in the Febbraio lab. I had no part in collecting or analyzing this data; it was used with his permission to lay a foundation for the experiments that were performed by myself as part of this dissertation. Development of experiments and techniques was done in collaboration with Dr. Febbraio. In Chapter 3, I was responsible for all cell culture work, DNA and RNA collection for sequencing, and colorimetric plasma lipid analyses. Bone marrow transplants, and blood and tissue collection were performed with help from Dr. Febbraio and Dr. Alexiou. Aneesh Bhardwaj assisted in analyzing plasma chromatography lipoprotein profiles. Dr. Omar and Dr. Febbraio collaborated on sequencing data analysis and interpretation, as well as editorial and intellectual contributions to this dissertation.

All animal procedures were approved by the University of Alberta Animal Care and Use Committee under animal use protocol # 570 (Febbraio; approved in 2013 and renewed in 2017).

Dedication

This thesis, and all the work put into it is dedicated to my both parents, Mrs. Agnieszka Lehmann and Mr. Andrzej Lehmann, my brother Thomas, and all my extended family living in Poland.

Acknowledgements

I would like to begin by expressing my appreciation and thanks to my supervisor, Dr. Maria Febbraio, for her unmatched mentorship in research since my first year of university. Your guidance and supervision have made me a better person, student, and scientist, and has convinced me to pursue research as part of my clinical practice in the future. I would like to recognize my committee members, Dr. Ava Chow and Dr. Liran Levin, for their invaluable insights, time spent at committee meetings, and guidance throughout my graduate studies. I would also like to acknowledge Dr. Stephane Bourque (external arm) for his time and insights, and Dr. Maryam Amin (chair) for her time as part of the examining committee for this dissertation.

A big thank you to my all fellow lab members: Dr. Maria Alexiou, Dr. Mohamed Omar, Dr. Umar Rekhi, Danielle Clark, Dr. Dongdong Fang, Aneesh Bhardwaj, Zahra Mantaka, Dr. Yuli Berlin-Broner, Dr. Linnet Immaraj, Julia Piche, Karen Ho, and Dr. Raisa Catunda for all your support throughout my graduate studies. It was a pleasure working with all of you throughout my many years in the lab. Thank you to all my other friends and colleagues in the Biomedical Oral and Maxillofacial Research Unit, as well in the DDS program, for your support throughout my graduate studies as well. Thank you to Dr. Shokrollah Elahi, Garrett Dunsmore, and Dr. Afshin Namdar Mehdiabadi for their mentorship and assistance in performing flow cytometry experiments. A final thank you to all the funding sources without which my studies would not be possible: CIHR, The Faculty of Medicine and Dentistry, and the School of Dentistry (Fund for Dentistry Grant), and The Heart and Stroke Foundation.

Table of Contents

List of Tables

List of Figures

Figure 14. Genes involved in plasma catabolism and trafficking of lipids are differentially methylated and regulated in *Pg* recipient mice

List of Abbreviations

Apo - apolipoprotein

bp - basepair

BMDM – bone marrow-derived macrophages

CVD – cardiovascular disease

DMP – differentially methylated promoter

DMR – differentially methylated region

DMSO – dimethyl sulfoxide

DMEM - Dulbecco's Modified Eagle Media

ETC – electron transport chain

FACS – fluorescence-activated cell sorting

FBS – fetal bovine serum

FDR – false discovery rate

FPKM - fragments per kilobase of transcript sequenced per millions of base pairs sequenced

FPLC – fast protein liquid chromatography

GO – gene ontology

Gy – Gray

HDL – high-density lipoprotein

HFD – high fat diet

HSC – hematopoietic stem cells

IDL – intermediate low-density lipoprotein

IL – interleukin

IP – intra-peritoneal

IMDM - Iscove's Modified Dulbecco's Media

kb - kilobase

KO – knockout

LCCM - L929 Conditioned Cell Media

LDL – low-density lipoprotein

LDLR – low density lipoprotein receptor

mRNA-seq – mRNA-sequencing

NHANES 1 - First National Health and Nutrition Examination Survey

O_2^- - superoxide anion

oxLDL – oxidized LDL

p_{adj} – adjusted p-value

PBS – phosphate buffered saline

PCR – polymerase chain reaction

Pg - *Porphyromonas gingivalis*

ROS – reactive oxygen species

RPMI - Roswell Park Memorial Institute

SEM – standard error of mean

VLDL – very low-density lipoprotein

WGBS – whole genome bisulfite sequencing

WT - wildtype

List of Symbols

♂ - male

♀ - female

CHAPTER 1

Introduction

1.1 Cardiovascular disease

Cardiovascular disease (CVD) is currently one of the leading causes of death worldwide, accounting for approximately 17.8 million deaths in 2017 alone[1], the most of any health-related issue that year. In the preceding decade, the CVD mortality rate increased by a staggering 21.1%[1], even with the advent of lipid-lowering drugs and continuing research into understanding of the etiology and pathophysiology of the disease. This highlights not only its continued impact on the general health and wellbeing of society, but also the heavy strains it places on our healthcare systems financially. In the most recent report put out by the Public Health Agency of Canada on economic costs for disease, CVD accounted for approximately 13.6 billion dollars in direct medical costs and lost productivity in 2010 alone, having the highest hospital and drug expenditures of any chronic disease[2]. These high costs are not only true of Canada, but worldwide, including the European Union, where estimated costs reach a staggering 169 billion euros[3]. Thus, continued research into CVD prevention and treatment are critical to lessening its burden on our health care systems.

CVD describes a wide range of vascular diseases, with the greatest proportion of CVD-related deaths and morbidity reported due to myocardial infarctions (or heart attacks) and strokes[1]. CVD is a complex and multifactorial disease, highlighted by a long list of risk factors[4] which can make treatment extremely difficult. The Framingham Heart epidemiological study[5,6] has been indispensable in identifying these health-related risk factors, and associating them with increased CVD prevalence and incidence. These risk factors include hyperlipidemia[7,8], hypertriglyceridemia[9,10], diabetes[11], and smoking[12], all of which guide the screening and treatment of susceptible patients in practice today. On a basic level, these risk factors promote atherosclerosis, which is the underlying etiology for many CVD cases seen clinically.

Atherosclerosis is a chronic inflammatory condition of the arteries. It is characterized by the development of sub-endothelial plaques, which in advanced stages can lead to luminal occlusion, resulting in partial or complete blockage of perfusion of essential organs such as the heart and brain.

1.2 Pathophysiology of Atherosclerosis and Foam Cell Formation

Atherosclerosis initiation and progression is largely believed to be associated with risk factor-driven injury and dysfunction of the endothelial layer of arteries[13,14]. Endothelial dysfunction is a phenomenon characterized by two phenotypic changes that alter endothelial homeostasis. The first is impaired vasodilatory properties of the endothelium[15-17] altering vascular compliance, which acts synergistically with increased expression of pro-inflammatory, thrombotic and chemotactic factors[16,17] to promote a vascular microenvironment conducive to inflammatory cell migration and subendothelial lipoprotein retention[18,19]. This underlies the formation of initial fatty streak lesions, characterized by the formation of lipid-rich foam cells[20].

Foam cells are formed when macrophages, recruited into the subendothelial space by endothelial signalling, and activated by lipoprotein retention, become cholesterol-rich by uptake of subintimal-retained low-density lipoprotein (LDL) cholesterol[20]. LDL particles are derived from their predecessor, very low-density lipoprotein (VLDL). VLDL, produced by the liver, is mainly made up of triglycerides and cholesterol, and serves as one of the body's primary mechanisms for tissue lipid delivery. At sites of need, triglycerides are liberated from VLDL by the action of cellular lipases[21], turning the particle into its more cholesterol-enriched derivative, LDL. In this form, it is amiable to macrophage uptake[22,23], after which processing of the cholesterol leads to formation of a cholesterol droplet in the cytoplasm.

Normally, LDL cholesterol uptake and droplet size are tightly regulated together by the low density lipoprotein receptor (LDLR) pathway[24]. Thus, cytoplasmic cholesterol excess promotes various cholesterol efflux pathways[25,26]. The primary objective of these pathways is to remove cholesterol through association with apolipoprotein (Apo) A1 or a high-density lipoprotein (HDL) particle; these particles are responsible for cholesterol clearance, by delivering excess back to the liver for excretion (reverse cholesterol transport)[27].

Macrophage foam cells, which initiate atherosclerosis lesion formation, can form in pathological states as a result of cholesterol accumulation despite this regulatory feedback.[28,29]. This is because modified forms of LDL bypass the normal LDLR mode of entry and utilize alternative pathways. These pathways are not bound by intracellular cholesterol regulation in the same way as the LDLR pathway, and involve the uptake of oxidized LDL (oxLDL)[30]. This modified form of LDL is generated by oxidative stress and overproduction of reactive oxygen species (ROS) by many cell types in atherosclerotic initiation, including activated endothelium and pro-inflammatory M1 macrophages[31,32]. Thus, the combination of LDL particles in an oxidative environment is a key etiological factor promoting foam cell formation, and thus atherosclerotic lesion development.

Fatty streaks are subclinical vascular lesions that do not produce signs or symptoms. These occur at a basal rate in most people, and in the context of a Western diet, can even be found in early childhood[33,34]. They rely on the risk factor-mediated elaboration of endothelial dysfunction and inflammation to progress. Lesion progression involves further foam cell formation, recruitment of other immune cell types (including T cells[35] and B cells[36]), as well as formation of a fibrous cap from extracellular matrix production by vascular smooth muscle cells[37]. Normally, vascular remodelling in these early progressed lesions prevents any symptomatic clue of their

presence[38]. However, as plaques grow, continued inflammation, combined with foam cell apoptosis and immune cell necrosis, leads to thinning of the fibrous cap, and formation of a pro-thrombotic core that promotes plaque rupture[39]. Release of these pro-thrombotic agents into the circulation leads to clot formation, occlusion of arteries, and ischemia of vital organs.

Various risk factors are responsible for promoting the formation and progression of atherosclerotic lesions. One risk factor that has been gaining some attention in the scientific community in the last two decades has been periodontitis; many epidemiological and observational studies support periodontitis as an independent risk factor for CVD[40-43].

1.3 Periodontitis

Periodontitis is an inflammatory disorder of the periodontium, the support apparatus of our teeth including the periodontal ligament, gingiva, and alveolar bone[44]. Inflammatory responses to bacterial biofilms on teeth of genetically or medically susceptible hosts leads to loss of gingival connective tissue attachment, followed by alveolar bone loss, which in the most severe cases can lead to tooth hypermobility, and even loss[45]. While the periodontal biofilm is a network of diverse species[46], there are certain bacteria that have been highly associated with increased periodontitis-mediated destruction, including bacteria of the Red Complex: *Porphyromonas gingivalis* (*Pg*), *Treponema denticola,* and *Tannerella forsythia*[47]. These bacteria possess a number of adaptations that allow them to thrive in in subgingival environment, where immune responses against these bacteria and others in the biofilm initiate inflammation characteristic of periodontitis[44]. These species derive energy using anaerobic metabolism[48,49], equipping them to survive in the low-oxygen environment subgingivally. Various virulence factors inherent to these bacteria also aid in their survival. *Pg*-encoded gingipains amplify inflammation[50] and promote adhesion of *Pg* to

epithelium, thus allowing it to colonize the subgingival environment[51]. In combination with its ability to evade the immune system by resisting killing by innate immune mechanisms such as oxidative burst[52] and complement[53], *Pg* can persist in subgingival plaques, which is key to its role as a keystone pathogen, coined for the ability of *Pg* to alter biofilm dynamics and promote increased biofilm virulence[54].

Damage due to periodontitis, even if treated non-surgically and deemed stable, is irreversible, and leaves patients with a reduced periodontium unless invasive surgery is undertaken. Beginning in 1999, periodontitis was described broadly by four major categories: chronic, aggressive, necrotizing, and due to systemic diseases[55]. Based on this classification, chronic periodontitis was associated with an older cohort of patients, high amounts of plaque and calculus, and a slow to moderate rate of progression[56]. Aggressive periodontitis was much quicker in progression, found at higher incidence in younger populations, and the amount of periodontal damage often did not correlate with the amount of plaque seen clinically[56]. However, population research over the last two decades and clinical case analyses have deemed it difficult to differentiate between the chronic and aggressive forms, and they are now combined under a periodontitis diagnosis scheme based on stage (the severity of disease) and grade (rate of progression), as well as a patient's diabetes and smoking status[57,58].

1.4 The Association Between Periodontitis and Cardiovascular Disease

A number of hypotheses have been developed regarding the mechanistic basis for the association between the periodontitis and CVD. Because both diseases are defined by an inflammatory component, the predominant hypothesis is that the response to periodontal pathogens, such as *Pg*, combines synergistically with vascular inflammation induced by CVD risk factors to increase atherosclerosis[59,60]. Various meta-analyses and clinical studies have shown

inflammatory markers of oxidative stress, as well as interleukin (IL)-6, and C-reactive protein, to be increased systemically in periodontitis patients[61,62]. These mediators are known to have crucial roles in the development of atherosclerosis and CVD[63,64]. In addition to systemic inflammation, the presence of periodontal pathogens in atherosclerotic plaques has led some to believe that periodontitis promotes bacteremia and direct pathogen involvement in the vascular microenvironment leading to an enhancement of atherosclerosis[40,65].

One of the many questions surrounding this association is whether treatment of periodontitis can impact CVD risk. A ground-breaking study in 2001 investigating data from the First National Health and Nutrition Examination Survey (NHANES 1) showed that periodontitis patients made edentulous, and thus having clinical elimination of periodontitis, had the same elevated risk of suffering a CVD event due to coronary artery disease as those with periodontitis[66]. The stunning thing about this observation is that it was made at a 17 year follow up of the study's participants. Other studies looking at long-term risk comparing edentulous and dentate periodontitis patients have found a reduced risk, but not a total reduction. In an analysis of cerebrovascular disease and non-hemorrhagic stroke risk, patients made edentulous had a lower risk of incidence or mortality, but residual risk was present and elevated above periodontally-healthy controls[67]. Similar observations were made for coronary heart disease events, with studies finding edentulous individuals having either similar risk to periodontitis patients[68], or the presence of a residual risk above healthy controls under the age of 60[69]. These studies suggest that total reversal of CVD risk is often not fully realized, even in the absence of periodontitis or chronic dental infection.

The theme of persistent risk is not one limited to periodontitis. One of the other major risk factors for CVD is smoking. It has been shown that smoking contributes to atherosclerosis development by various mechanisms, including increasing vascular oxidative stress[70] and oxLDL

production[71], promoting a pro-atherogenic serum lipid (characterized by increased VLDL and LDL, with decreases in HDL)[72], and increasing vascular inflammation[73]. In studies of heavy smokers who successfully achieve cessation of their habit, it has been noted that they continue to an elevated risk of suffering a heart attack twenty years after quitting[74]. Another pertinent example is that of diabetes. As with smoking, one of the main hypotheses surrounding its association involves a chronic systemic inflammation, brought on by insulin resistance[75,76]. Studies have also supported diabetic hyperglycemia acting on serum lipids, with glycation of serum lipoproteins not only promoting increased LDL oxidation[77], but also impairing HDL function[78]. Persistent risk in diabetics with atherosclerosis has also been reported, as those who are able to achieve normoglycemia have higher risk of developing heart attacks and strokes years after controlling their blood glucose[79,80]. In all the cases above, the immune system plays a key role in the pathologies observed clinically.

1.5 DNA Methylation in Inflammatory Disease

One of the key controlling factors of immune cell phenotype and inflammation is epigenetic modification. While the cellular epigenetic landscape is vast, one of the most common is DNA methylation. This form of epigenetic change involves covalent attachment of methyl groups to cytosine, which alters the affinity of the DNA for nucleosomes[81], but also directly alters binding of transcriptional factors to their regulatory sequences[82], providing cells with a way of tightly controlling the availability of binding sites for various transcription and regulatory factors along the lengths of genes. The methylation level of a gene is dependent on the interplay between DNA methyltransferases, which place methyl groups, and DNA demethylases, which remove them, leading to hypermethylation or hypomethylation of genes, respectively[83]. DNA methylation, and epigenetic changes as whole, are key regulators of cell phenotype, as they are reversible, and

control gene expression in a sequence-independent manner[84]. These properties are critical in imparting phenotypic plasticity, allowing cells to integrate the cues and stimuli in their immediate environment into a functional transcriptional response. This is particularly true in chronic inflammatory states. In conditions such as systemic lupus erythematosus and rheumatoid arthritis, DNA methylation changes have been identified that amplify the inflammatory response and promote disease pathogenesis[85,86]. Atherosclerosis and periodontitis, the two associated chronic diseases of interest in this dissertation, are no exception.

In atherosclerosis studies using hypercholesterolemic mouse models, elevated blood lipids have been shown to promote DNA methylation changes in the bone marrow progenitor and hematopoietic stem cell populations; when these cells were transplanted, they promoted monocytosis (elevated blood monocytes) and elevated atherosclerosis[87]. Dietary by-products of inflammation, including oxLDL, have been shown to moderate DNA methylation of pro-atherogenic genes[88]. Risk-factor promoted inflammation has become a hot topic in atherosclerotic research, with studies identifying changes in the methylation of various genes as having a potential association with increased risk of developing CVD[89]. Importantly, in mouse studies using DNA methylation inhibitors, the reversal of some pro-atherogenic changes was noted, reducing foam cell and plaque formation, and thus solidifying epigenetic changes as another therapeutic avenue to consider in the future[90].

The role of DNA methylation in periodontitis, just as in atherosclerosis, has been shown to be important in disease development. Studies of gingival biopsies and blood leukocytes from periodontitis patients have uncovered differential expression of a number of genes encoding pro-inflammatory cytokines, including IL–6[91], tumor necrosis factor - α[92], and interferon – γ[93] due to changes in promoter methylation. Periodontal pathogens, including *Pg*, have been shown to have

the ability to induce changes in DNA methylation that may promote periodontitis progression[94]. Pilot studies looking at the ability of periodontitis treatment to reverse disease-promoting methylation of pro-inflammatory genes have found reversal, but also maintenance of methylation patterns post treatment, significant in potential for future relapse of periodontitis[95]. The important role of DNA methylation in promoting atherosclerosis and periodontitis necessitates further exploration into the impact epigenetic changes can have in promoting disease long-term.

1.6 Hypothesis, Aims and Objectives

After treatment of an inflammatory disease such as periodontitis, any risk for developing associated diseases such as CVD should diminish with continuous turnover of the immune system. The turnover of immune cells occurs on the orders of days to weeks[96,97], nowhere near the 17 year timeline observed in the prospective study of the NHANES 1 data on periodontitis and CVD risk[66]. The fact that this risk remains elevated for such a long period of time suggests that there may be a mechanism, a form of memory, that might be perpetuating changes in the immune cells that are pro-atherogenic.

Our lab hypothesizes that one mechanism at play involves long-term epigenetic changes induced during periodontitis, occurring in self-renewing hematopoietic stem cells (HSC) in the bone marrow. HSC are the stem cell of the immune system, possessing key self-renewing capabilities[98] that allow for immune system maintenance and turnover. Combined with the intrinsic property of epigenetic changes to be passed between cells during division and development[99], epigenetic changes would persist in the bone marrow, for years upon years, even after elimination of periodontitis. In effect, persistence of epigenetic changes in the bone marrow would lead to

long-term reprogramming of immune cells, including macrophages, which are known to have extensive roles in both periodontitis and atherosclerosis.

The objective of my studies was to investigate DNA methylation changes induced in HSC and progenitors during chronic *Pg* infection in the context of a hyperlipidemic, CVD mouse model (LDLR knockout (KO)), to determine if epigenetic re-programming of the immune system during periodontitis has a role in persistent CVD risk. I used a bone marrow transplant approach with two syngeneic donor mouse cohorts. One was orally infected with *Pg* while the other was sham-infected with vehicle. The bone marrow from both donor cohorts was transplanted into separate healthy, irradiated syngeneic mice. This model mimics a situation whereby any *Pg*-induced changes in the bone marrow should be passed to the recipients, but the mouse is otherwise healthy and free from the direct effects of *Pg* infection. Differences in DNA methylation in bone marrow progenitor cells were compared to differences in gene expression in bone marrow-derived macrophages (BMDM) and associated with plasma lipid analyses to determine if changes in immune cell phenotype can have systemic effects promoting atherosclerosis.

CHAPTER 2

Materials and Methods

2.1 Cell Media Recipes

2.1A. Iscove's Modified Dulbecco's Media (IMDM) (for flushing bone marrow cells)

- IMDM (ThermoFisher Scientific - #12440053)
- 10% heat inactivated (55°C waterbath for 2 hours) fetal bovine serum (FBS; Hyclone - SH 30396.03)
- 100 U/mL penicillin and 100 µg/mL streptomycin (Hyclone – SV30010).

2.1B. Bone Marrow Transplant Media

- IMDM
- 100 U/mL penicillin and 100 µg/mL streptomycin

2.1C. Dulbecco's Modified Eagle Media (DMEM) L929 Growth Media

- DMEM (Hyclone – SH 30081.01)
- 10% heat inactivated FBS
- 100 U/mL penicillin and 100 µg/mL streptomycin
- 2 mM L-glutamine (Sigma – G7513)

2.1D. L929 Conditioned Cell Media (LCCM)

- LCCM was made using DMEM L929 Growth Media (recipe 2.1C above). When L929 cells were grown to near confluency in an initial 10 mL volume of DMEM L929 Growth Media, they were supplemented with an additional 10 mL without replacement for an additional 10 days. The final 20 mL supernatant collected was LCCM (see section 2.2.12 for details).

2.1E. Bone Marrow Resuscitation Media

- Roswell Park Memorial Institute (RPMI) media (Hyclone – SH 30255.01)
- 10% heat inactivated FBS
- 100 U/mL penicillin and 100 µg/mL streptomycin
- 2 mM L-glutamine

2.1F. BMDM Differentiation Media

- RPMI
- 10% heat inactivated FBS
- 100 U/mL penicillin and 100 µg/mL streptomycin
- 2 mM L-glutamine
- 15% LCCM

2.1G. Progenitor Flush Media

- Ca^{2+}, Mg^{2+}, biotin free phosphate buffered saline (PBS, made from 10X stock; Hyclone - SH30258.01)

- 2% heat inactivated FBS
- 1 mM EDTA (Fisher Scientific – 46-034-CI)

2.1H. Fluorescence-activated cell sorting (FACS) buffer

- Sterile, Ca^{2+}, Mg^{2+}, biotin free PBS
- 2% heat inactivated FBS

2.1I. FACS Blocking Buffer

- Ca^{2+}, Mg^{2+}, biotin free PBS
- 2% heat inactivated FBS
- 20% Rat Serum (STEMCELL – 13551)

2.1J. Progenitor Expansion Media

- StemSpan™ Serum-Free Expansion Medium (STEMCELL – 09650)
- 100 U/mL penicillin and 100 µg/mL streptomycin
- 2 mM L-glutamine
- 40 µg/mL human LDL (STEMCELL – 02698)
- 10 ng/mL mouse recombinant IL-3 (STEMCELL – 78042.1)
- 10 ng/mL human recombinant IL-6 (STEMCELL – 78050.1)
- 50 ng/mL mouse recombinant stem cell factor (STEMCELL – 78064.1)

2.2 Experimental Methodology

Please note: All recipes for the various types of media used are outlined in section 2.1

2.2.1 Mice

All animal procedures were approved by the University of Alberta Animal Care and Use Committee under animal use protocol # 570 (Febbraio). All animals were housed and cared for by the University of Alberta Health Sciences Laboratory Animal Services. Studies were done using LDLR KO male mice from Jackson Laboratories (Strain #002207; B6.129S7-*Ldlr*^{tm1Her}/J). These mice develop atherosclerotic lesions concomitant with the feeding of a high fat diet (HFD)[59,100,101].

2.2.2 Periodontitis Mouse Model

All studies used an experimental mouse model of periodontitis involving oral infection with *Pg*. This model has been used extensively by investigators in the field, and has been shown to induce alveolar bone loss and a systemic cytokine and antibody response[102-104]. Oral infection with *Pg* was accomplished by modification of a previously described protocol[105]. Briefly, ~$2x10^9$ colony forming units/mL *Pg* were resuspended in 2% sterile carboxymethylcellulose (a food thickener to promote bacterial adherence). Mice were infected by oral lavage, by application of *Pg* using a microbrush into each of the 4 quadrants of the dentition (previously *Pg* was introduced with a micropipette). Mice were infected every other day for two weeks. Mice were euthanized at 16-20 weeks by pentobarbital overdose.

2.2.3 *Pg* cultivation

Pg was purchased from ATCC (strain #33277). Bacteria were grown in Schaedler's broth (Oxoid - #CM0497) supplemented with 1% Vitamin K_1 + Hemin (BD Bioscience - #212354) under anaerobic conditions (Mitsubishi AnaeroPack™ 2.5L anaerobe jar – ThermoScientific R685025; AnaeroPack™ - Anaero Anaerobic Gas Generator – ThermoScientific R681001) for 24-48 hours. Cultures grown to saturation were centrifuged @ 20,000 x *g*. Pellets were resuspended in 2% sterile carboxymethylcellulose made in saline.

2.2.4 Bone Marrow Donor Cohorts

Male LDLR KO mice 6-8 weeks old were randomly assigned to one of two bone marrow donor groups. Mice in the first group were infected with *Pg* orally as described in 2.2.2; mice in this group will henceforth be referred to collectively as *Pg* donors. Mice in the second group received 2% sterile carboxymethylcellulose applied by lavage as a control and will be known as the sham donors. Prior to lavage, mice were anesthetized to surgical plane by intra-peritoneal (IP)

injection of a ketamine-xylazine cocktail at doses of 100 mg/kg and 10 mg/kg, respectively. Concomitant with the first instance of lavage in both groups, mice were fed a HFD (Envigo Teklad #88137) for 16-20 weeks prior to bone marrow transplantation. This diet is 21% fat by weight and contains 0.15% cholesterol, and has been used extensively to promote development of atherosclerosis in LDLR KO mice[100,101].

2.2.5 Bone Marrow Recipient Cohorts

After a minimum of 16 weeks HFD feeding to induce atherosclerosis, bone marrow was harvested from donor mice from both cohorts for transplantation. Bone marrow was transplanted into 12-week-old healthy, irradiated LDLR KO male mice. Mice receiving bone marrow from *Pg* donors will be known as *Pg* bone marrow recipients; those with transplanted bone marrow from sham donors will be known as sham bone marrow recipients.

2.2.6 Mouse Irradiation and Bone Marrow Transplantation

Recipient mice were irradiated using a split dose protocol, 2 x 5.5 Gray (Gy) for a total dose of 11 Gy from a Cesium-137 source (Gammacell 1000 Elite irradiator, Alberta Diabetes Institute Core Facility). The time of irradiation (T) necessary to generate 5.5 Gy of radiation was calculated according to the following formula:

$$T = \frac{Desired\ Central\ Dose\ (Gy)}{\left(Central\ Dose\ Rate\ [\frac{Gy}{min}]\right) * Decay\ Factor}$$

Central dose rate, or the amount of Cesium-137 released per unit time, was 11.53 Gy/min. The decay factor was a function of the Cesium-137 half-life and changed depending on the date of transplant. Once calculated, 5.5 Gy was administered twice, 4 hours apart, and mice were rested for 2 hours prior to transplantation.

During this time, *Pg* and sham donor mice were euthanized with IP injection of pentobarbital at a dose of 200 mg/kg (BiMeda-MTC Animal Health Inc, 00141704). Hind limbs were surgically removed, and cleaned of skin, muscle, and connective tissue. The tibia and femur were then detached at the knee joint to allow for separate processing of each bone. Bones were pierced by a 25-gauge needle at either end, and marrow was flushed with a 25-gauge needle connected to a 1cc syringe, by passing IMDM media for flushing (solution 2.1A) several times through the bones, until they were clear of cells. Cells (~$2x10^7$/donor mouse) were centrifuged (5 minutes @ 3783 x *g*) and resuspended at a concentration of ~10^7 cells/mL in bone marrow transplant media (solution 2.1B).

An equal volume of donor bone marrow was transplanted into 4-5 recipient mice/donor mouse by retroorbital injection (~$5x10^6$ donor cells/mouse). Recipient mice were then fed normal chow (4% fat by weight) for the remainder of the experiment.

2.2.7 Progenitor and Stem Cell Isolation

The first set of experiments performed aimed at analyzing hematopoietic progenitor methylomes in both the *Pg* and sham donor bone marrows. For progenitor isolation, bone marrow was flushed as described in 2.2.6, however with progenitor flush media (solution 2.1G), for compatibility with the EasySep™ Mouse Hematopoietic Progenitor Cell Isolation Kit (STEMCELL – 19856). Isolation was then carried out according to the manufacturer's instructions. Briefly, following flush, bone marrow was centrifuged (10 minutes @ 300 x *g*) and resuspended in 500 µL of fresh progenitor flush media. Bone marrow cells were then mixed and incubated with two kit components. The first was an antibody cocktail (STEMCELL – 19856C) capable of binding non-progenitor bone marrow cell markers (CD5, CD19, B220, Ly6G, TER119, 7-4; added at 50 µL/mL of sample). This step negatively selected for the bone marrow progenitor

population, by having antibodies bind various terminal immune cell populations. In addition, rat serum (STEMCELL – 50001) was added to block non-specific antibody binding to surface Fc receptors. Incubation with antibodies and rat serum lasted 15 minutes at 4°C. Cells were further incubated with RapidSpheres™, magnetic beads that had the capability to sequester antibody-bound cells, for 10 minutes at 4°C, at a concentration of 75 µL/mL of sample. The volume of the cell suspension was then increased to 2.5 mL with progenitor flush media and placed in an EasySep™ magnet (STEMCELL – 18000) for 3 minutes. This allowed cells bound to magnetic beads to be sequestered out of solution. The remaining solution, containing the purified hematopoietic progenitors, was poured off. Magnet sequestration of immune cells was repeated once more, after which purified cells were counted using a hemocytometer, and cultured.

2.2.8 Stem Cell and Progenitor Culture

Following isolation, the purified progenitors were cultured, to expand the populations for whole genome bisulfite sequencing (WGBS) and methylome analysis. Expansion of the stem cell/progenitor population was done according to previously published protocols[106]. Briefly, $2x10^4$ progenitor cells were plated in 6 wells of a 24-well tissue culture plate (Corning – 353047) in 1 mL of progenitor expansion media (solution 2.1J). Fives days after initial plating, coincident with cell confluency, cells were lifted by gentle pipetting, and split 1:3 in 666 µL of fresh progenitor expansion media and 333 µL of the 1 mL used to initiate culture on day 1. After splitting, cells were grown in culture until day 8.

2.2.9 Progenitor DNA Isolation

Eights days after initiating progenitor culture, cells were removed from plates by gentle pipetting, and centrifuged (5 minutes @ 870 x *g*). Cells were then resuspended in progenitor flush media (solution 2.1G) and passed through the EasySep™ Mouse Hematopoietic Progenitor Cell

Isolation Kit to remove any other cell types that may have been generated during culture (section 2.2.7). Isolated progenitor cells were then resuspended in 200 µL of PBS for the purpose of genomic DNA extraction using the PureLink® Genomic DNA Mini Kit (Invitrogen – K1820-01). Briefly, cells were incubated with Proteinase K and RNase A (both at 1.67 mg/mL) for 2 minutes at room temperature. Cells were then mixed with a lysis/binding buffer and incubated at 55°C for 20 minutes to promote RNA and protein digestion. The lysate was then mixed with 200 µL of 100% ethanol**,** vortexed, and moved to a spin column. The binding buffer and ethanol promoted DNA binding to the silica membrane, and when the lysate was centrifuged (10,000 x *g* for 1 minute), most of the contaminating cellular components were removed. Two further washes were used to remove contaminants, with one centrifugation between them (10,000 x *g* for 1 minute), and one at the end (20,184 x *g* for 3 minutes) to remove any residual wash buffer and contaminants in the spin column. Spin columns were then placed into sterile microfuge tubes, and DNA was eluted in Tris-HCl (10 mM) – EDTA (0.1 mM) buffer by centrifuging at 20,184 x *g* for 1 minute.

2.2.10 Internal DNA Quality Control

2.2.10.1 Non-denaturing agarose gel electrophoresis

To ensure that isolated progenitor DNA met the standards for purity and integrity required for WGBS, non-denaturing agarose gel electrophoresis was performed. Briefly, 200 ng of DNA was added to sterile PCR water, and DNA loading dye (ThermoFisher Scientific – R0611). DNA was loaded and electrophoresed on a 1% agarose gel with a final concentration of 0.85 µM ethidium bromide (ThermoFisher Scientific – BP1302 – 10). The GeneRuler 1 kilobase (kb) DNA ladder (ThermoScientific – SM1331) was loaded for molecular weight determination. Samples were electrophoresed at a constant amperage (15 mA) for 25 minutes. Gels were imaged using the ChemiDoc™ MP Imaging System (Bio-Rad) and analyzed in Image Lab 5.0 software (Bio-Rad).

DNA was considered usable if it was free from protein and RNA contamination, and no visible smearing indicating degradation was observed.

2.2.10.2 Qubit® Fluorometric Analysis and Nucleic Acid Spectrophotometry**.**

To supplement purity analysis by gel electrophoresis, 1 µL of DNA was analyzed by a NanoDrop™ 2000 spectrophotometer (ThermoScientific) by assessment of A_{260}/A_{280}. A ratio of ~1.8 was considered pure DNA. Genomic DNA concentration was quantified by fluorometric analysis using the Qubit® 2.0 Fluorometer system (ThermoScientific) in conjunction with the Qubit™ dsDNA High-Sensitivity Assay Kit (ThermoScientific – Q32854). Briefly, 1 µL of sample was added to 199 µL of a working solution containing a fluorescent nucleic acid binding reagent selective for dsDNA in Axygen PCR-05-C tubes (VWR – 10011-830). Samples were vortexed and incubated at room temperature for 3 minutes prior to reading. All Qubit®-based nucleic acid quantifications were performed at the University of Alberta Faculty of Medicine & Dentistry Applied Genomics Core (TAGC), which receives financial support from the Faculty of Medicine & Dentistry and Canada Foundation for Innovation awards to contributing investigators.

2.2.11 Methylome Analyses

All sequencing, sample preparation, bioinformatic analyses, and quality control were performed by Novogene Co. Ltd (https://en.novogene.com/next-generation-sequencing-services/gene-regulation/whole-genome-bisulfite-sequencing/).

2.2.11.1 WGBS

Genomic DNA was fragmented to 200-400 base pair (bp) sequences. Ends were repaired and adenylated, providing an overhang for adaptor ligation. The DNA was then bisulfite-treated twice. This treatment converted non-methylated cytosines into uracil (read as thymine during

sequencing), while methylated cytosines were retained. Fragments in the 200-400 bp range were amplified by polymerase chain reaction (PCR) and used to generate libraries for sequencing. Sequencing was performed on the Novaseq6000 Illumina® platform, generating 150 bp paired end reads. By comparing bisulfite-treated fragments to the mouse reference genome (*Mus musculus*; ftp://ftp.ensembl.org/pub/release-93/fasta/mus_musculus/dna/), methylated and unmethylated cytosines were mapped.

2.2.11.2 Data Quality Control

Prior to data analysis, reads were processed according to the following 5 parameters:

A. Sliding Window Approach. Each raw read was scanned in 4 bp increments, removing any sequences containing poor quality reads.
B. Leading and Trailing. Poor quality bases, or those that could not be read, at the 5' and 3' end of read were trimmed.
C. Illumina Clip. Adaptor sequences ligated for sequencing were removed.
D. Minimum Length Trimming. Reads below a minimum length of 36 bp were removed from the pool of reads.
E. After the trimming steps from A-D were performed, if any unpaired reads remained, these were discarded.

2.2.11.3 Read Mapping and Data Analysis

Clean reads were mapped to the mouse reference genome using Bismark software (0.12.5)[107]. Methylation level at a single-nucleotide resolution was determined as the ratio of methylated and total (methylated and unmethylated) cytosines at a position. Following analysis of methylation level, differentially methylated sites were identified using Fisher's exact test and p-

value was adjusted (p_{adj}) using false discovery rate (FDR) multiple test correction. Sites with $p_{adj}<0.05$ and a difference of more than 0.2 in methylation level between the *Pg* and sham samples were considered differentially methylated. Differentially methylated regions (DMR) were considered candidates if $p_{adj}<0.05$ (Fisher's exact test; FDR multiple corrections). Finally, differentially methylated promoters (DMP) were localized to 2000 bp upstream of each gene and were considered significant by the statistical parameters used for DMS.

2.2.12 Production of LCCM

L929 cells were purchased from ATCC (NCTC clone 929 [L cell, L-929, derivative of strain L] (ATCC® CCL-1™)). This extensively used and well-defined cell line releases proteins and growth factors which promote the differentiation of macrophages from total bone marrow[108]. Cells were resuscitated and expanded in DMEM L929 growth media (solution 2.1C) on tissue culture coated T75 flasks (ThermoFisher Scientific - 156472). Initial expansion of cells was done in 10 mL of this media; cells were fed as needed to confluency. At confluency, 2 mL of 0.25% trypsin-EDTA (Gibco - 25200-072) was used to detach cells from the flask, and cells were passaged 1:5 into new T75 flasks for LCCM (solution 2.1D) production. At passage, cells were plated in 10 mL of DMEM L929 growth media, and at near confluency were further supplemented with 10 mL of media (without replacement). L929 cells were then cultured for 10 days before supernatant was collected, sterilized through a 0.2 µm filter, aliquoted and stored at -20°C until needed.

2.2.13 Generating BMDM

Sham and *Pg* recipients were sacrificed by IP injection of pentobarbital at a dose of 200 mg/kg. The tibia and femur were removed, cleansed of tissue, and flushed in IMDM flushing media as before. Flushed bone marrow cells were centrifuged out of suspension (5 minutes @ 3783 x *g*),

and frozen in 90% FBS and 10% dimethyl sulfoxide (DMSO) at ~$1x10^7$ cells/cryovial. Cells were placed in -80°C for 24 hours, before being preserved in liquid nitrogen.

BMDM were generated according to protocols published elsewhere[108]. Briefly, when needed, frozen total bone marrow cells were resuscitated by thawing at 37°C gently, and then resuspended in 9 mL bone marrow resuscitation media (solution 2.1E) to dilute out DMSO. Media was added dropwise along the wall of the tube. Cells were centrifuged (5 minutes @ 870 x *g*), and pelleted cells were resuspended in 10 mL BMDM differentiation media (solution 2.1F). Cells were plated on 100 mm bacterial plastic dishes. On day 4 after initial culture, 10 mL of additional BMDM differentiation media was added without replacement to the culture, and macrophages were allowed to grow to confluency.

2.2.14 F4/80 expression assessment of BMDM

To ensure our protocol to differentiate macrophages from bone marrow was effective, expression of F4/80, a pan macrophage marker, was measured by flow cytometry. LCCM was removed from the culture dish and replaced with 4 mg/mL lidocaine hydrochloride (Sigma - CAS73-78-9) made in 1X PBS. After a 10-minute incubation at room temperature, cells were lifted by gentle pipetting, and centrifuged at 870 x *g* for 5 minutes. Cells were washed once with sterile PBS, and aliquoted into V bottom plates (Costar - 3897) at $1x10^6$ cells/100 µL of FACS buffer (solution 2.1H). Non-specific antibody binding was blocked by a 15-minute incubation of cells in FACS blocking buffer (solution 2.1I) at room temperature. Cells were then incubated with anti-mouse F4/80-Alexa Fluor 488 antibody (Life Technologies - MF48020, 1:100) made in FACS buffer for 30 minutes, at room temperature, in the dark. Cells were washed twice in 100 µL of FACS buffer and fixed in 4% paraformaldehyde (ThermoFisher Scientific - 28908) for 10 minutes at room temperature. Cells were washed once with 100 µL of FACS buffer after fixation and

resuspended in 250 µL PBS. Flow cytometry was performed using the Attune NXT Flow Cytometer (ThermoFisher Scientific) using the parameters of the BL1 laser (Excitation: 488nm; Emission: 530/30 nm). All flow cytometry experiments were performed at the University of Alberta Faculty of Medicine & Dentistry Flow Cytometry Facility, which receives financial support from the Faculty of Medicine & Dentistry and Canada Foundation for Innovation awards to contributing investigators.

2.2.15 RNA isolation from Recipient BMDM

To determine if differences in DNA methylation identified in donor progenitors correlated with changes in transcription post-transplant, recipient BMDM were processed for RNA after reaching confluency. Briefly, BMDM differentiation medium was removed from confluent cultures and replaced with 4 mg/mL lidocaine hydrochloride made in PBS. Lidocaine is one of the extensively used methods for detaching macrophages grown on bacterial plastic[109,110]. Cells were incubated for 10 minutes at 37°C, before being lifted by gentle pipetting. After being centrifuged (5 minutes @ 870 x *g*) from lidocaine, cells were washed once in PBS. After centrifugation (5 minutes @ 870 x *g*) to remove PBS, cells were lysed and homogenized in 1 mL of TriZol Reagent (Invitrogen – 15596026) by repeated pipetting. Samples were then frozen at -80°C in anticipation of RNA isolation.

RNA was prepared using TriZol reagent following a protocol modified from the manufacturer's instructions. Upon reaching room temperature after thawing, 200 µL of molecular biology-grade chloroform (ThermoFisher Scientific – BP1145- 1) was added per 1 mL of TriZol. Samples were mixed gently by inversion and incubated on ice for 5 minutes. The aqueous (RNA–containing), interphase (DNA-containing), and organic (protein-containing) layers were separated by centrifugation (12,000 x *g* for 15 minutes at 4°C). The uppermost aqueous phase was removed,

mixed with 500 µL of 2-propanol (Sigma Aldrich – 19516), and incubated at room temperature for 10 minutes. Following incubation, RNA was pelleted by centrifugation (12,000 x *g* for 15 minutes at 4°C). RNA was then washed 3 times with RNase-free 70% ethanol, centrifuging (7500 x *g* for 5 minutes at 4°C) and decanting the wash buffer each time. RNA was then allowed to dry for approximately 5-10 minutes, before being resuspended in RNase-free water. Secondary RNA structure was denatured by incubation at 55°C for 10 minutes prior to freezing RNA samples at -80°C.

2.2.16 Assessment of RNA Quality

2.2.16.1 Non-denaturing agarose gel electrophoresis

RNA purity and integrity were measured by non-denaturing agarose gel electrophoresis as described in section 2.2.10.1 with the following adaptations:

- 400-600 ng of RNA was loaded per sample
- Samples were electrophoresed at constant voltage (70V) for 45-60 minutes.
- RNA was considered acceptable if it was free from protein and DNA contamination, and the 28S:18S ratio was ~2:1.

2.2.16.2 Qubit® Fluorometric Analysis and Nucleic Acid Spectrophotometry

Qubit® and NanoDrop™ RNA analyses were performed as described for DNA previously (section 2.2.10.2) with the following adaptations:

- An A_{260}/A_{280} of ~ 2 was considered pure for RNA
- The kit used for fluorometric RNA quantification was the Qubit™ RNA HS Assay Kit (ThermoFisher Scientific – Q32852).

2.2.17 mRNA-sequencing (mRNA-seq)

mRNA-seq, transcriptome analyses, and further quality control measures were performed by Novogene Co. Ltd (https://en.novogene.com/next-generation-sequencing-services/gene-regulation/mrna-sequencing-service/)

2.2.17.1 Library Preparation and Quality Control

Transcriptome cDNA libraries were prepared generally by mRNA enrichment, RNA fragmentation, and cDNA synthesis using random hexa-primers. Adaptors were ligated to ends, and cDNAs between 250-300 bp were amplified by PCR. Sequencing was performed using Illumina® Next Generation sequencing technology, utilizing paired sequencing of 150 bp from each side of the cDNA.

To ensure quality of our sequencing data, reads used for downstream analyses were first filtered from the raw pool of reads based on the follow characteristics:

i. Reads did not have adaptors still ligated.
ii. Reads had <0.1% of bases that could not be read.
iii. Reads were of good quality overall.

2.2.17.2 Transcriptome Analysis

Clean reads were then aligned to the *Mus musculus* reference genome (GRCm38/mm10) using STAR (v2.5) software. The number of times each gene was read, and expression level was measured using FPKM (fragments per kilobase of transcript sequenced per millions of base pairs sequenced), taking into account the number of reads that were mapped, the gene length, and the sequencing depth. Based on the FPKM values calculated, differential gene expression analysis was

performed. Resulting p-values were adjusted by the Benjamini-Hochberg method to control for FDR, and a p_{adj} <0.05 was set to define genes that were differentially expressed. Genes identified were then organized based on gene ontology (GO; http://www.geneontology.org/), roles in biological systems (KEGG; http://www.kegg.jp/), and pathway and reaction involvement (Reactome; http://www.reactome.org). Statistically-significant enrichment was considered when p_{adj}<0.05 (Benjamini – Hochberg FDR correction).

2.2.18. Mouse Plasma Collection

Mice were fasted overnight for 16-18 hours prior to plasma collection. *Pg* and sham recipient mice were euthanized by IP injection of 200 mg/kg pentobarbital. A 1cc syringe was coated with 0.05M EDTA – $2K^+$, and EDTA was loaded to a final concentration of 5 mM when ~1 mL of blood was collected by cardiac puncture. Total blood was centrifuged (3783 x *g* for 5 minutes) to separate erythrocytes, leukocytes, and plasma. Plasma was collected, aliquoted, and stored at -20°C, or used immediately for lipoprotein analyses.

2.2.19. Lipoprotein Analyses

All lipoprotein analyses were performed by the Lipidomics Core Facility, part of the Faculty of Medicine and Dentistry at the University of Alberta, Edmonton, Canada, which receives financial support from the Faculty of Medicine & Dentistry, the Women and Children's Health Research Institute, and Canada Foundation for Innovation awards to contributing investigators. The distribution of plasma cholesterol and triglycerides among the VLDL, LDL, and HDL fractions were measured using fast lipoprotein chromatography (FPLC)[111,112]. Briefly, plasma (15 µL for cholesterol analysis; 27 µL for triglyceride analysis) was injected by autosampler into an Agilent 1200 HPLC instrument that was outfitted with a Superose 6 HR 10/300 gel-filtration FPLC

column. This system separated intact lipoproteins based on size. An in-line assay for total cholesterol (Cholesterol-SL reagent from Sekisui Diagnostics – 234-60) or triglycerides (Triglyceride-SL reagent from Sekisui Diagnostics – 236-60) was performed using post-elution reactions at 37°C. Reactions were monitored in real-time at 505 nm, with data analysis performed using Agilent ChemStation software.

The representative areas under the curves for VLDL, LDL, and HDL were calculated. Differences between *Pg* and sham recipients were statistically compared by Mann-Whitney U analysis, where significance was set at $p<0.05$. All statistical analyses were performed using GraphPad Prism software (Version 5.0).

2.2.20 Cholesterol and Triglyceride Analysis

In addition to lipoprotein analyses, plasma was analyzed by validated colorimetric kits from FujiFilm Wako Diagnostics U.S.A for total cholesterol (#99-02601) and triglyceride (#290-63701), as well as free cholesterol (#993 – 02501). Esterified cholesterol was extrapolated by subtracting the free, non-esterified cholesterol from the total cholesterol measured for each replicate.

To measure total cholesterol, 2 μL of plasma was mixed with a buffer solution containing a number of enzymes. Cholesterol ester hydrolase was present to release cholesterol from its esterified form bound to fatty acids. Together with the already free cholesterol, newly released cholesterol was oxidized by cholesterol oxidase to form hydrogen peroxide. In the presence of peroxidase, 3,5–dimethoxy-N-ethyl-N-(2-hydroxy-3-sulfopropyl)-aniline sodium salt, and 4-aminoantipyrine, hydrogen peroxide participates in a reaction to form a blue pigment, measured by absorbance at 600 nm. Absorbance was measured using a Synergy™ H1 Microplate Reader

(BioTek) 5 minutes after mixing plasma and buffer solution. Reactions were monitored and analyzed using Gen 5 2.07 software (BioTek). To measure the proportion of free cholesterol in plasma, cholesterol oxidase reaction was used to form hydrogen peroxide in the same manner as for total cholesterol. Total triglyceride was measured by combining 2 μL of plasma with a buffer containing, among other components, lipoprotein lipase. This enzyme breaks down triglycerides into its principal components, glycerol and fatty acids. Glycerol kinase then converts glycerol into glycerol-3-phosphate, which is oxidized by glycerol-3-phosphate oxidase to form hydrogen peroxide and produce blue pigment as above.

Differences between *Pg* and sham recipients in plasma levels of these different parameters were statistically compared by unpaired t-test (if samples passed the D'Agostino & Pearson omnibus normality test) or Mann-Whitney U analysis, where significance was set at $p<0.05$. All statistical analyses were performed using GraphPad Prism software (Version 5.0).

CHAPTER 3

Results

3.1 Control bone marrow irradiation/transplant experiment demonstrates protocol efficacy

This experiment, as well as those in sections 3.2-3.4, were performed prior to me starting my MSc. I was not involved in any part of these experiments, but I cite them here as the rationale for my experiments. To ensure the efficacy of the irradiation protocol (outlined in section 2.2.6) used for ablation of native recipient bone marrow, we performed a control bone marrow transplant experiment using CD36 KO donors and wildtype (WT) recipients. This was necessary because our transplants involved syngeneic donor and recipient LDLR KO mice, and thus immune cell phenotypes could not be differentiated post-transplant. After gating monocytes on the CD11b^{+}/CD11c^{-} subset (Fig. 1A), they were stained for CD36 expression. Non-transplanted, WT controls showed a CD36^{+} monocyte population of 18.6% in the blood (Fig. 1B). Following transplant of WT mice with

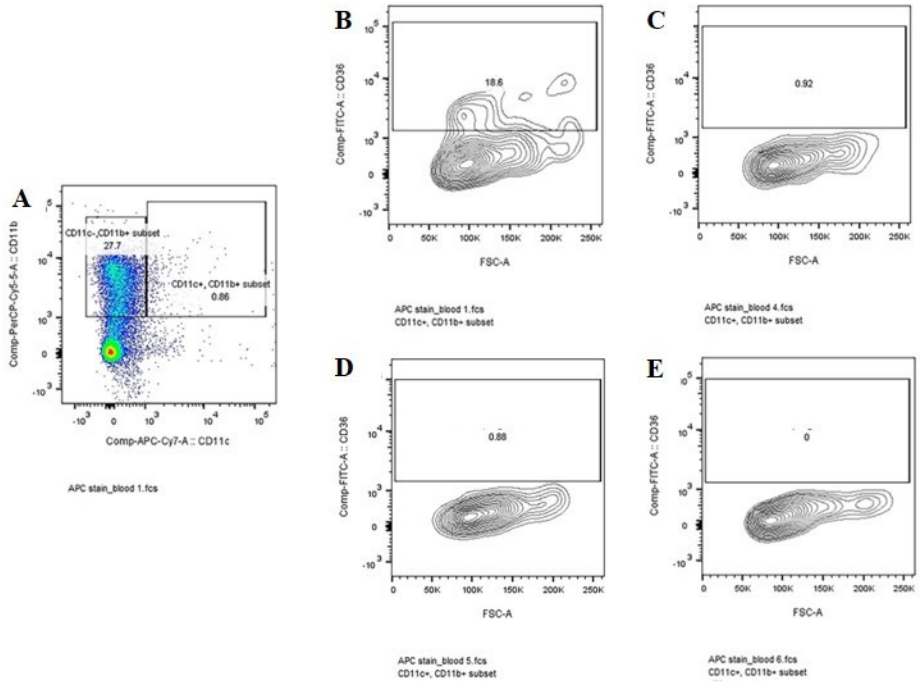

Figure 1. Recipient irradiation protocol is sufficient for ablation of native bone marrow cells. WT mice were irradiated with a 2 x 5.5 Gy (11 Gy total) 4 hours apart and transplanted with bone marrow from CD36 KO mice. Whole blood was collected, and leukocytes isolated by Ficoll paque gradient separation. Resultant cells were incubated with antibodies for CD11b, CD11c, as well as CD36 and subjected to flow cytometry. **A.** Monocytes were gated based on CD11b expression and lack of CD11c expression. **B.** CD36 expression on WT monocytes from a WT control mouse. **C-E.** Three independent transplant recipients showing monocyte CD36 expression following CD36 KO bone marrow transplant into WT recipients.

CD36 KO bone marrow, the percent CD36$^+$ monocyte populations dropped below 1% in three independent transplants (Fig. 1C-E), representing ~95% decrease in CD36$^+$ monocytes in recipient mice.

3.2 *Pg* recipient mice displayed an increased atherosclerotic lesion burden, with significant differences observed primarily in male mice

LDLR KO recipient mice were irradiated and transplanted with bone marrow from *Pg* or sham donor mice. Following the reconstitution phase, in which the recipients were fed normal chow for 4 weeks, to allow for turnover of circulating blood cells, the mice were fed a HFD for 16 weeks to promote atherosclerosis (LDLR KO mice do not develop atherosclerotic lesions unless fed a HFD). *Pg* recipient mice displayed a 38% increase in atherosclerosis in the aorta as measured by aortic morphometry (Fig. 2A; $p<0.05$). When mouse sex was taken into account, only male *Pg* recipient mice showed a significant increase (63%) in atherosclerotic lesion burden compared to their sham counterparts (Fig. 2B; $p<0.05$); the increase observed in female *Pg* recipient mice was not significant (Fig. 2B).

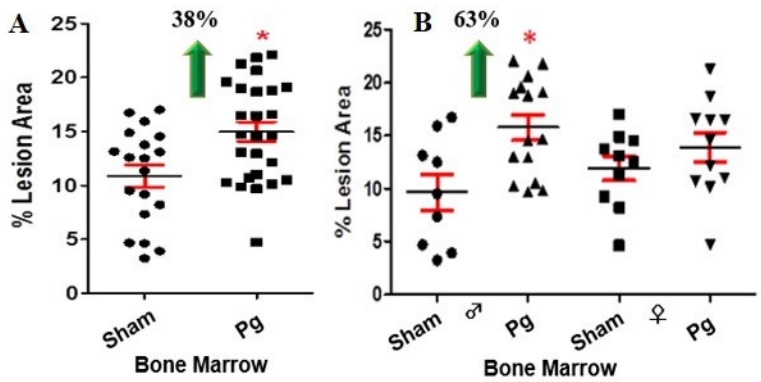

Figure 2. Recipient mice receiving *Pg* and sham donor bone marrow show differences in atherosclerotic burden after HFD feeding. **A.** Recipient mice were fed a HFD for 16 weeks, after which aortas were dissected, stained with oil red O and atherosclerotic lesion area determined by aortic morphometry. **B.** Atherosclerotic lesion burden compared when results in (A) were divided into male (♂) and female (♀) cohorts. In both figures, one point represents one mouse. Data is presented as mean ± standard error of mean (SEM) and was analyzed by unpaired t-test (* indicates $p<0.05$).

3.3 Donor mice did not display differences in total plasma cholesterol or weight

Sham and *Pg* bone marrow donor mice of both sexes were assessed for differences in weight and total plasma cholesterol, potential confounding factors that could impact bone marrow stem cell phenotype. Both male and female *Pg*-infected bone marrow donor mice did not display any differences in weight (Fig. 3A) or total plasma cholesterol (Fig. 3B) when compared to their sham counterparts.

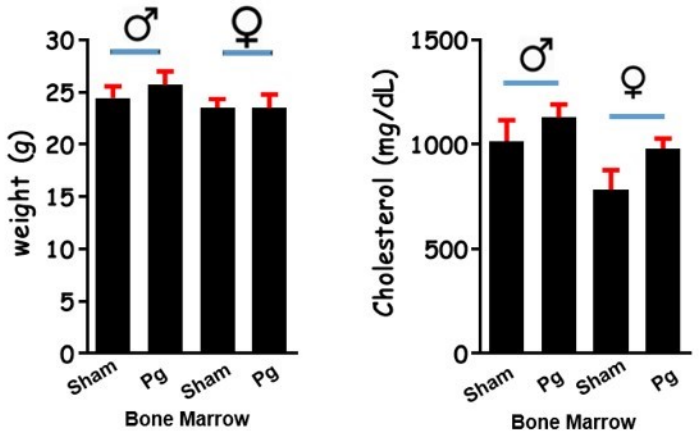

Figure 3. Donor mice do not show differences in total cholesterol or weight pre-transplant. At time of sac for transplant, male (♂; sham N=9 and *Pg* N=15) and female (♀; sham N=10 and *Pg* N=11) mice were weighed (**A**) and blood was collected for plasma cholesterol analysis by colorimetric assay (**B**). Data is presented as mean ± SEM with analysis between *Pg* and sham donor cohorts done by unpaired t-test.

3.4 *Pg* recipient-derived macrophages display differences in promoter methylation, with an elevated pro-inflammatory cytokine profile

The differences in aortic atherosclerosis observed only between *Pg* and sham recipient male mice (Fig. 2B) prompted the lab to continue using male mice to investigate a potential epigenetic underpinning to these results. Following transplant, peritoneal macrophages elicited from both recipient groups were sent for WGBS methylome analysis. In these studies (Fig. 4A), differences in gene promoter methylation were observed between the *Pg* and sham recipient groups. These results further prompted initial studies investigating differences in macrophage phenotype. With atherosclerosis being a chronic inflammatory disease, inflammatory status of

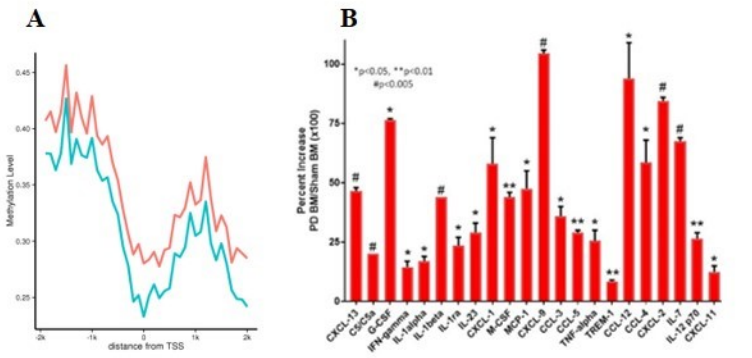

Figure 4. Macrophages from *Pg* recipient mice display differences in promoter methylation, as well as a more pro-inflammatory cytokine profile. Macrophages were elicited by thioglycollate injection twenty weeks post transplant. Macrophage genomic DNA was pooled (N=5/group) and sent for whole genome bisulfite sequencing (**A**), where promoter methylation level was assessed at a single nucleotide resolution 2 kb upstream and downstream of the transcription start site (TSS). Blue line represents analysis of *Pg* recipient mice; red line represents the sham recipients. In addition, pooled lysates (N=5/group; normalized for protein) were analyzed for global cytokine expression by chemiluminescent membrane array (**B**). This system measures cytokine protein levels as a function of chemiluminescent intensity. Data is presented as mean ± SEM, and as a ratio between the intensities of *Pg* recipient macrophages (labelled as PD BM) to sham recipient macrophages (labelled as sham BM). These ratios were then converted to percentage values. Groups were compared by unpaired t-test; *p<0.05, **p<0.01, #p<0.005.

recipient macrophages was measured by global cytokine array; macrophages elicited from *Pg* recipient mice displayed a more pro-inflammatory cytokine repertoire overall (Fig. 4B). This major finding, combined with the initial WGBS data obtained, gave support to a *Pg* infection-mediated epigenetic reprogramming of HSC, promoting increased atherosclerosis in *Pg* recipient mice post-transplant (Fig. 2B). To build on these studies, the research in this dissertation eliminated epigenetic pressure of the HFD in the recipients. Placing recipients on normal chow allowed the lab to attribute phenotypes and DNA methylation changes observed in recipients to donor *Pg* infection.

3.5 Systemic triglyceride levels are elevated in *Pg* recipient mice, with no differences in weight or total plasma cholesterol

Post-transplant, male recipients were fed normal chow to remove the potential pressure from the HFD. Eight months post-transplant, *Pg* and sham mice did not show differences in weight (Fig. 5C). Total plasma cholesterol (Fig. 5A) was slightly higher in the *Pg* recipients (219.6 ± 21.0 mg/dl) compared to those from the sham group (194.1 ± 18.38 mg/dl), but the difference

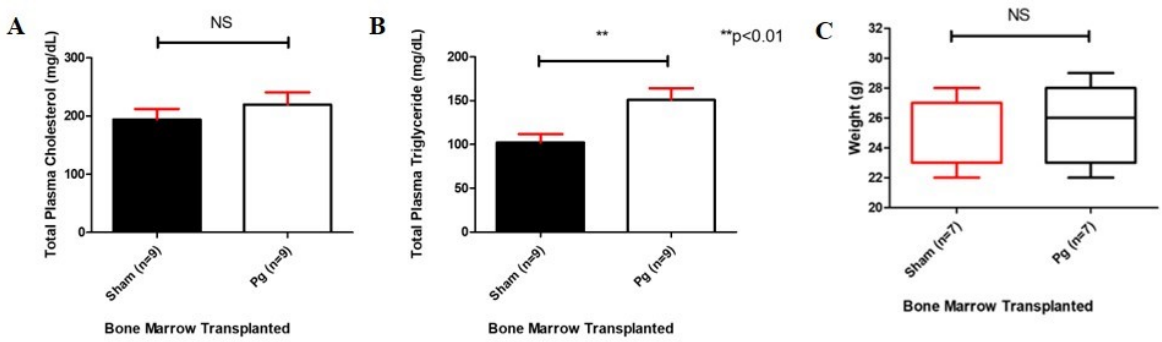

Figure 5. *Pg* recipient mice do not display any differences in weight or total plasma cholesterol but show increased plasma triglyceride concentration. Plasma was isolated from whole blood collected by cardiac puncture 8 months post-transplant, and total plasma cholesterol (**A**) and triglyceride (**B**) concentrations were determined by colorimetric assay (N=9/ group for both analyses). Cohorts were compared by unpaired t-test (** indicates p<0.01; NS indicates non-significant), and data is presented as mean ± SEM. **C**. At time of blood collection, mice were also weighed (N=7/group), and groups were compared by Mann-Whitney U test.

was not statistically significant (p>0.05). Interestingly however, there was a significant increase in plasma triglycerides in the *Pg* recipients (151.0 ± 13.1 mg/dl versus 102.3 ± 9.5 mg/dl; p<0.01; Fig. 5B).

3.6 Plasma HDL and esterified cholesterol were significantly different in *Pg* recipient mice

In addition to total plasma cholesterol, we also measured two other cholesterol attributes. The first were the proportions of total cholesterol that was present in the esterified (covalently bound to fatty acid) or free (or unesterified) forms. *Pg* recipients displayed significantly higher amounts

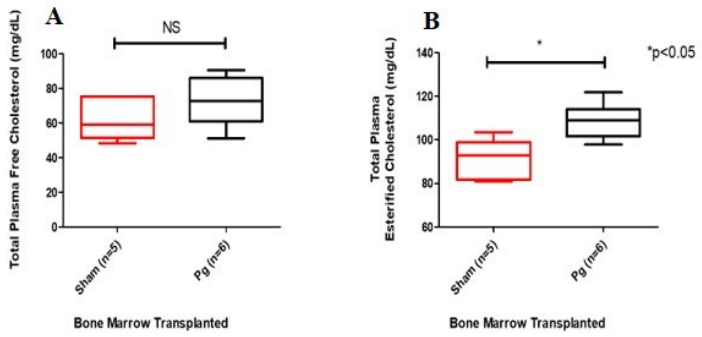

Figure 6. *Pg* recipient mice show differences in total plasma esterified, but not free, cholesterol. Plasma collected from whole blood by cardiac puncture was assessed for free (not bound to triglyceride; **A**) and esterified (bound to triglyceride; **B**) cholesterol levels. N=5 for sham recipients; N=6 for *Pg* recipients. Groups were compared by Mann-Whitney U test (* indicates p<0.05; NS indicates not significant).

of esterified cholesterol (Fig. 6B; $p<0.05$), however did not show any differences in free

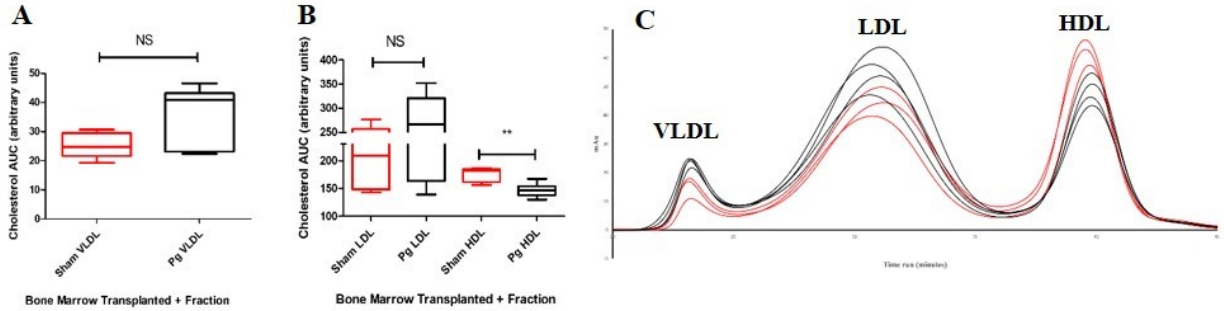

Figure 7. Cholesterol distribution in plasma lipoproteins of recipient mice. Plasma lipoproteins were separated by FPLC, and total cholesterol was quantified by calculating the area under the curve (AUC) of their respective peaks (N=6 for sham; N=7 for *Pg*). Cholesterol for VLDL is in (**A**), and those for LDL and HDL (both in **B**). Statistical analysis was performed using the Mann-Whitney U test (**indicates $p<0.01$; NS indicates not significant). **C.** Representative FPLC results from 1 of 2 experiments: *Pg* (black; N=4) and sham (red; N=3) recipient mice. Three characteristic peaks are present: VLDL (quickest to elute), LDL, and HDL (slowest to elute). Time of elution is on the x-axis; milli-Absorbance units (mAu) from spectrometric analysis is on the y axis.

cholesterol (Fig. 6A). The second property analyzed was the distribution of cholesterol in various plasma lipoprotein: VLDL, LDL and HDL (Fig. 7C). No significant differences were observed in VLDL (Fig. 7A) and LDL (Fig. 7B), however the amount of cholesterol in the HDL fraction was significantly less ($p<0.01$) in the *Pg* recipient mice (Fig. 7B).

3.7 Triglyceride is significantly increased in VLDL of *Pg* recipient mice

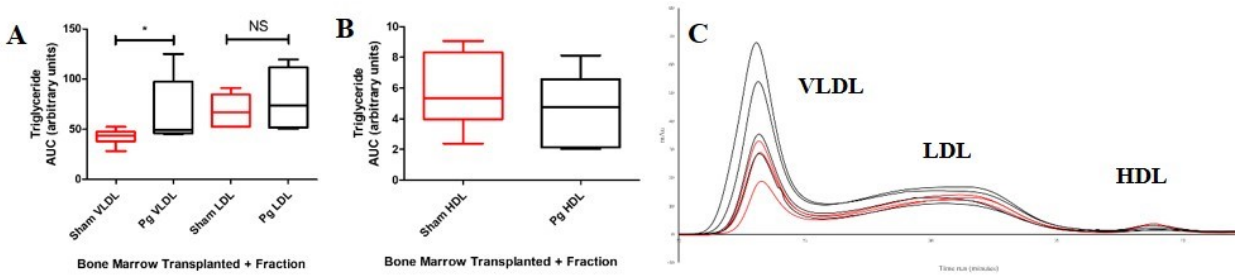

Figure 8. Triglyceride distribution within lipoprotein fractions of recipient mice. Plasma lipoproteins were separated by FPLC, and total triglyceride was quantified in each eluted fraction. Triglyceride in VLDL and LDL (both **A**), as well as HDL (**B**), were quantified by calculating AUC of their respective peaks (N=6 for sham; N=7 for *Pg*). Statistical analysis was performed using the Mann-Whitney U test (*indicates $p<0.05$; NS indicates not significant). **C.** Representative curves from 1 of 2 experiments; *Pg* (black; N=4) and sham (red; N=3) recipient mice. Three characteristic peaks are present: VLDL (quickest to elute), LDL, and HDL (slowest to elute). Time of elution is on the x-axis; milli-Absorbance units (mAu) from spectrometric analysis is on the y axis.

Analyzing the distribution of triglycerides in plasma VLDL, LDL and HDL (Fig. 8C), *Pg* recipient mice showed increased triglycerides in VLDL ($p<0.05$; Fig. 8A), but not the LDL (Fig. 8A) or HDL (Fig. 8B) fractions.

Table 1. Descriptive information about *Pg* and sham donor bone marrow progenitor samples sequenced by WGBS

Sample	Raw Bases/ Raw Base Production (Gb)	Clean Base Production (Gb)	Sample	Total Reads	Unique Mapped Reads	Unique Mapping rate (%)	Sequencing depth
WD1	380,891,454 /57.1	54.8	99.89	186,868,174	145,114,528	77.66	13.53
WD2	288,841,610 /43.3	41.7	99.93	141,805,753	107,097,884	75.52	9.84
WD3	253,686,500 /38.1	36.6	99.94	125,119,774	92,117,958	73.62	8.3
WDPg1	244,248,446 /36.6	35.4	99.94	120,857,246	91,916,003	76.05	8.27
WDPg2	241,541,970 /36.2	34.1	99.89	119,572,330	94,622,096	79.13	8.27

Sample abbreviations are as follows: sham (n=3) – WD1, WD2, and WD3; *Pg* (n=2) – WDPg1, WDPg2.

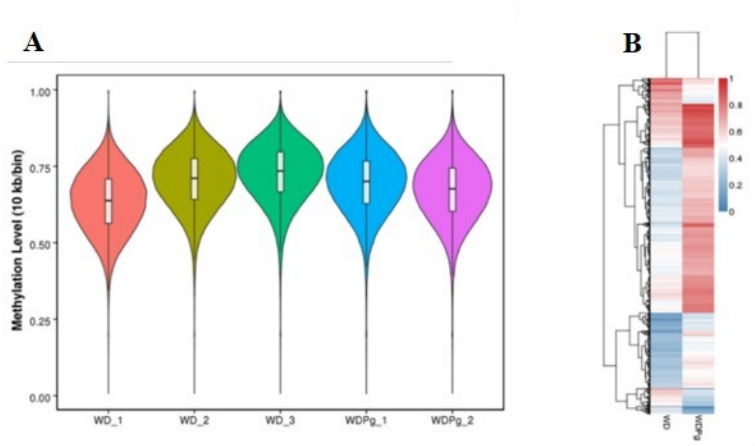

Figure 9. Global genome methylation and gene specific methylation in *Pg* and sham donor mice. **A.** Using 10 kb bins, the methylation level was calculated based on the ratio of methylated cytosines to the total (methylated and unmethylated) cytosines within each bin. Each violin plot is displayed as a box plot indicating the median with respective 25% and 75% interquartile ranges. The number of 10 kb bins with a certain methylation level is indicated by the width of the Violin plot. Sample abbreviations: sham (N=3) - WD1, WD2, and WD3; *Pg* (N=2) - WDPg1 and WDPg2 **B.** Cluster analysis of DMP. Promoter methylation is presented as a continuum from red (hypermethylation) to blue (hypomethylation).

3.8 Donor Bone Marrow Progenitor WGBS Analysis

To begin cataloging DNA methylation differences induced in *Pg* donor mice, and identify differences promoting atherosclerosis and lipid phenotype observed in Figures 5-8, bone marrow progenitor cell DNA from *Pg* and donor mice was isolated and sent for WGBS analysis (Novogene). Descriptive information about the *Pg* (WDPg; N=2) and sham (WD; N=3) samples sequenced are presented in Table 1. Raw base sequencing data generated across samples varied from approximately 241,000,000 – 380,900,000 (36.2 Gb – 57.1

Gb) reads, with 34.1 – 54.8 Gb being filtered as clean base reads, and thus used for mapping to the genome. Bisulfite conversion was greater than or equal to 99.89% in all samples. On average, approximately 76% of reads were uniquely mapped (i.e. only mapped once) to the *Mus musculus* genome. Sample sequencing depth varied between 8.27 and 13.53 but remained around the ~10x depth initially sought for each replicate. On a global level, progenitors from *Pg* donor mice as a group did not show statistically significant differences in global genome methylation (Fig. 9A). However, analysis at the gene level, specifically in DMP, showed skewing towards gene hypermethylation in the *Pg* donors (Fig. 9B).

3.9 Recipient BMDM Transcriptome Analyses

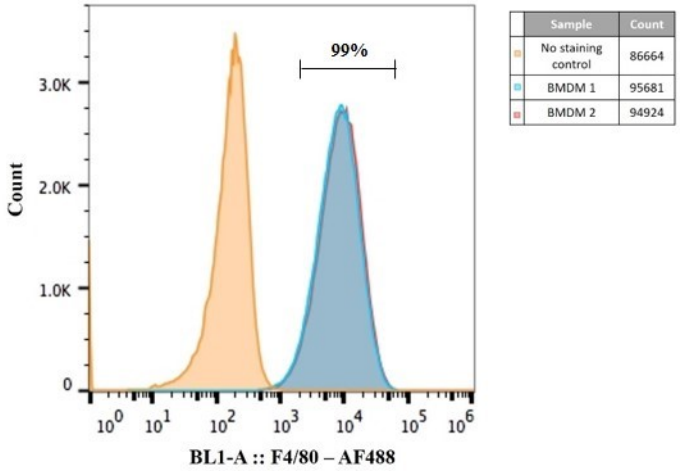

Figure 10. BMDM express the pan macrophage marker F4/80. Expression of F4/80 was assessed by flow cytometry. Following culture of total bone marrow in BMDM differentiation media, macrophages were stained for F4/80 expression (Excitation: 488nm; Emission: 530/30 nm). 100,000 cells/sample were counted. The orange histogram represents unstained controls; the blue and red histograms (overlapping) represent macrophages derived from the bone marrow of two independent mice. Approximately 99% of BMDM expressed F4/80 above the unstained control.

To correlate changes in DNA methylation with differential expression in macrophages, macrophages were differentiated from bone marrow progenitors isolated from recipient mice 8 months post-transplant and analyzed by mRNA-seq (Novogene). Macrophages were chosen for differential expression analysis owing to their important roles in the initiation of atherosclerosis[20]. Prior to RNA isolation, macrophage differentiation was assessed using the pan marker F4/80, as has been done in other studies using the L929 method for BMDM generation[108]. Flow cytometry analysis of BMDM showed approximately a two-log difference between unstained controls and

Table 2. Descriptive information about the *Pg* and sham recipient BMDM samples sequenced with RNAseq

Sample	Raw Bases/ Raw Base Production (Gb)	Total Reads	Clean Base Production (Gb)	Error Rate (%)	Uniquely Mapped Reads	Mapping rate (%)
rmWD_1	88,847,700/13.3	87,310,526	13.1	0.03	82,180,596	94.12
rmWD_1	82,158,622/12.3	80,728,962	12.1	0.02	75,920,788	94.04
rmWD_3	90,532,130/13.6	89,211,752	13.4	0.02	83,662,164	93.78
rmWDPg_1	82,003,092/12.3	80,868,578	12.1	0.02	76,817,352	94.99
rmWDPg_2	75,023,524/11.3	73,873,710	11.1	0.02	69,549,894	94.15
rmWDPg_3	93,958,456/14.1	92,414,346	13.9	0.02	87,413,510	94.59

Sample abbreviations: rm – recipient macrophages; sham N=3) – rmWD1, rmWD2, and rmWD3; Pg (N=3) – rmWDPg1, rmWDPg2, and rmWDPg3.

those stained for F4/80, with 99% of the BMDM staining positive for F4/80 above unstained controls in both independent replicates (Fig. 10). Descriptive information about sham (rmWD; N=3) and *Pg* (rmWDPg; N=3) data following mRNA-seq is found in Table 2. Raw base sequencing data produced between 75-94 million reads (11.3 – 14.1 Gb of data). Following filtering procedures there were 73.8 – 92.5 million clean reads, representing between 11.1 -13.9 Gb of data that was mapped to the mouse genome. Of the clean reads mapped, approximately 94% of them were uniquely mapped to a region of the genome across all replicates. Of the transcripts mapped to the genome, a total of 1358 genes were identified as differentially expressed in the *Pg* recipient BMDM (p_{adj}<0.05; Fig. 11), with 538 being upregulated, and 775 being downregulated.

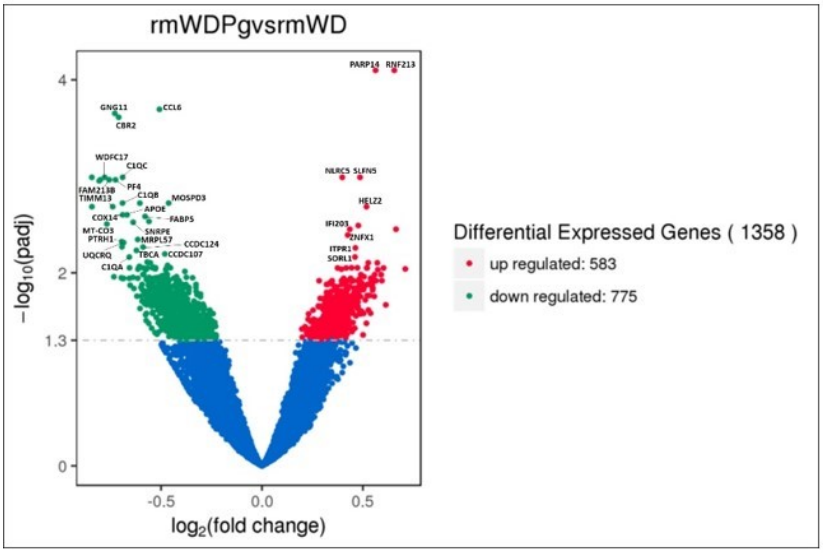

Figure 11. Volcano plot describing differentially expressed genes. Following comparison of BMDM mRNA sequencing data from *Pg* and sham recipient mice, those genes upregulated (in red) and those downregulated (in green) were plotted as a function of their fold change (expressed as $\log_2$ (fold change)) on the x-axis, and their p_{adj} (expressed as $-\log_{10}(p_{adj})$) on the y-axis. Genes not meeting p_{adj}<0.05 (corresponding to a $-\log_{10}$ value of 1.3) were not considered as differentially expressed and are presented in blue.

3.10 Macrophages derived from *Pg* recipient mice display transcriptional changes in oxidative metabolism and cell stress management

Following mRNA sequencing of data, differentially expressed genes were organized by bioinformatics analysis based on gene ontology and function (GO enrichment), and involvement in cellular pathways (reactome and KEGG analyses). In GO analysis (Table 3), interesting trends were observed regarding cell metabolism. Many of the top cellular functions involving differentially expressed genes had functions in ATP metabolism, purine metabolism, mitochondrial electron transport, as well as oxidative phosphorylation ($p<0.00005$). In addition, cell detoxification was significantly impacted by differential expression ($p<0.0005$). This was supported by the results of the reactome and KEGG enrichment, serving to group genes into functional pathways. KEGG analysis revealed a significant number of genes involved in oxidative phosphorylation ($p<5x10^{-18}$; Table 4). Reactome analysis indicated cellular responses to stress and detoxification of ROS as pathways significantly enriched in the differentially expressed gene population, ($p<0.05$; Table 4), in addition to genes involved in respiratory electron transport and the citric acid cycle ($p<5x10^{-8}$; Table 4).

Table 3. GO enrichment of differentially expressed genes in mRNA-seq

GO Enrichment ID	Cellular Function	p_{adj}
GO:0046034	ATP metabolic process	1.54E-08
GO:0009205	purine ribonucleoside triphosphate metabolic process	1.54E-08
GO:0009199	ribonucleoside triphosphate metabolic process	2.56E-08
GO:0009144	purine nucleoside triphosphate metabolic process	2.56E-08
GO:0009141	nucleoside triphosphate metabolic process	2.56E-08
GO:0009126	purine nucleoside monophosphate metabolic process	3.44E-08
GO:0009167	purine ribonucleoside monophosphate metabolic process	3.44E-08
GO:0022900	electron transport chain	5.42E-08
GO:0009161	ribonucleoside monophosphate metabolic process	5.49E-08
GO:0009123	nucleoside monophosphate metabolic process	2.62E-07
GO:0006119	oxidative phosphorylation	4.78E-07
GO:0010257	NADH dehydrogenase complex assembly	5.95E-07
GO:0032981	mitochondrial respiratory chain complex I assembly	5.95E-07
GO:0042773	ATP synthesis coupled electron transport	7.20E-07
GO:0033108	mitochondrial respiratory chain complex assembly	2.18E-06
GO:0022904	respiratory electron transport chain	2.36E-06
GO:0042775	mitochondrial ATP synthesis coupled electron transport	3.70E-06
GO:0051651	maintenance of location in cell	3.70E-06
GO:1902600	proton transmembrane transport	1.14E-05
GO:0098754	detoxification	2.52E-04

Table 4. Reactome and KEGG enrichment of differentially expressed genes in mRNA-seq

Reactome			
Reactome ID	Pathway	Genes Involved	p_{adj}
R-MMU-1428517	The citric acid (TCA) cycle and respiratory electron transport	44	1.86E-10
R-MMU-611105	Respiratory electron transport	28	1.16E-08
R-MMU-2262752	Cellular responses to stress	46	1.34E-2
R-MMU-3299685	Detoxification of Reactive Oxygen Species	9	4.16E-2
KEGG			
KEGG ID	Pathway	Genes involved	
Mmu00190	Oxidative phosphorylation	52	3.59E-18

3.11 Identifying differentially methylated and differentially expressed genes contributing to a pro-atherogenic phenotype

Table 5. Genes of interest identified in donor bone marrow progenitor and macrophage RNAseq analyses

Gene Name	Methylation Level (Pg relative to sham donors)	Fold Change (Pg recipients vs sham recipients)	p-value for differential expression
SLC23A2	Hypo	1.24	1.86E-2
PON2	Hyper	0.84	2.49E-2
ACC1	Hypo	1.35	1.75E-2
SORL1	Hypo	1.38	6.86E-3
APOE	Hyper	0.63	2.51E-3
CBR2	Hyper	0.61	2.44E-4
NPC2	Hyper	0.78	2.21E-2
ATP5O	Hyper	0.83	4.95E-2
ATP5F1	Hyper	0.82	2.63E-2

Following cross-referencing of the mRNA-seq and WGBS data, data mining was performed to identify genes with expression and methylation patterns supporting a pro-atherogenic macrophage phenotype. Genes indicated in green were hypermethylated; those in red were hypomethylated.

Based on the initial overall results from the GO enrichment (Table 3) and the KEGG and reactome analyses (Table 4), WGBS data from donor bone marrow progenitors was cross referenced with data from recipient BMDM mRNA-seq. Genes identified in both data sets, with correlations between methylation status and differential expressions were noted and data mining was performed to identify patterns consistent with promoting atherosclerosis. There were nine candidate genes identified involved in oxidative metabolism, regulation of ROS production, as well as lipid metabolism (Table 5). Those that were hypermethylated included *PON2, APOE, CBR2, NPC2, ATP5O, ATPF1* (Table 5). Those that were hypomethylated included *SLC23A2, ACC1,* and *SORL1* (Table 5). A more detailed display of the methylome analysis, including regions methylated is found in Table 6.

Table 6. Raw descriptive data of differentially methylated and expressed regions identified in WGBS

Gene Name/Chromosome Number and Description	Functional Gene Element (s) and Corresponding Chromosomal Region	Methylation Level Percent Difference (Comparing *Pg* to sham)	Fold Change in Expression (rmWDPg vs rmWD)	p_{adj} (for differential expressions analysis)
SLC23A2/2 Sodium-Dependent Vitamin C Transporter 2	Exon, UTR3 *132054745 - 132055299*	-18.2%	1.24	1.86E-2

PON2/6 Paraoxanase 2	Exon, Intron *5271502 - 5272755*	+24.0%	0.84	2.49E-2
ACC1/11 Acetyl-CoA Carboxylase 1	Exon, Intron, Promoter *84279808 - 84280402*	-18.3%	1.35	1.75E-2
	Intron *84271649 - 84271923*	-14.2%		
	Intron *84211287- 84211532*	-17.4%		
	Intron *84241657 - 84242454*	-20.2%		
	Exon, Intron *84245246 - 84246010*	-26.8%		
	Exon, Intron *84399268 - 84399634*	-35.9%		
SORL1/9 Sortilin-Related Receptor 1	Exon, Intron *42031869 - 42031976*	-22.8%	1.38	6.86E-3
	Intron *42122944 - 42123307*	-35.7%		
	Intron *42024507 - 42025055*	-16.7%		
	Intron *42121755 - 42121933*	-24.8%		

	Intron *42032339 - 42032636*	-18.7%		
	Intron *42034651 - 42035174*	-19.4%		
	Intron *42120902 - 42121411*	-20.0%		
APOE/7 Apolipoprotein E	Exon, Intron, UTR5, Promoter *19698308 - 19698939*	+47.9%	0.63	2.51E-3
CBR2/11 Carbonyl Reductase 2	Exon *120767327 - 120767537*	+20.9%	0.61	2.44E-4
NPC2/12 NPC Intracellular Cholesterol Transporter 2	Promoter *84773754 - 84774419*	+27.1	0.78	2.2E-2
ATP5O/16 ATP Synthase Peripheral Stalk Subunit OSCP	Intron *91851874 – 91852316*	+19.5%	0.83	4.95E-2
	Intron *91794214 – 91795367*	+43.8%		
	Intron *91852879 – 91853282*	+13.8%		
	Intron *91838393 – 91838799*	+13.9%		

ATP5F1 ATP Synthase Peripheral Stalk-Membrane Subunit B	Exon, Promoter *157409959 - 157411015*	+26.2%	0.82	2.63E-2

As an extension of Table 5, genes are localized to a chromosome and regions identified to be differentially methylated by bioinformatics analysis and are presented as the functional element of the gene they are contained in, as well as their nucleotide range. Methylation level is also presented as a percent difference comparing *Pg* bone marrow progenitors to sham bone marrow progenitors.

3.12 Macrophages from *Pg* recipient mice display methylation and expression changes consistent with a pro-oxidative phenotype

Following data mining of differentially methylated and expressed genes (Tables 5 and 6), genes impacting macrophage ROS production were noted to be enriched in *Pg* recipient mice (Fig. 12). Foam cell ROS production is a key characteristic that not only impacts cytoplasmic oxLDL levels[113], but also upon extracellular release, can oxidize LDL in the intimal environment, and amplify endothelial cell activation and immune cell infiltration into atherosclerotic plaques[114,115], resulting in further progression and increase in atherosclerotic plaque formation (Fig. 12). One of the major ROS-producing mechanisms cells, including macrophages, make use of involves dysregulated electron transport in the mitochondrial electron transport chain (ETC)[116]. Classically, the ETC is composed of 5 protein complexes (referred to colloquially as complexes I – V), with complex V encoding an ATP synthase. Its normal function lies in oxidative phosphorylation and metabolism, where it uses electron transfer to generate a proton gradient by which ATP synthase powers ATP production. *ATP5O* and *ATP5F1,* which were both hypermethylated and downregulated in the consolidated data (Table 5), encode the OSCP and B subunits of ATP synthase, respectively[117-119]. Downregulation of subunits of ATP synthase in cardiac disease has

recently been shown to increase mitochondrial superoxide anion (O_2^-) production[120] with concomitant increases in the proton gradient being suggested as the major mechanism for ROS generation[121]. Production of ROS in the ETC occurs primarily by complexes I and III[122], which is further aided by the hypermethylation and downregulation of a key anti-oxidant in the mitochondria, *PON2*. *PON2* encodes for paraoxanase 2, an enzyme that has been shown to be associated with complex III in the mitochondria[123]. In *PON2* deficiency studies, macrophages expressing lower levels of *PON2* were shown to produce elevated mitochondrial ROS,

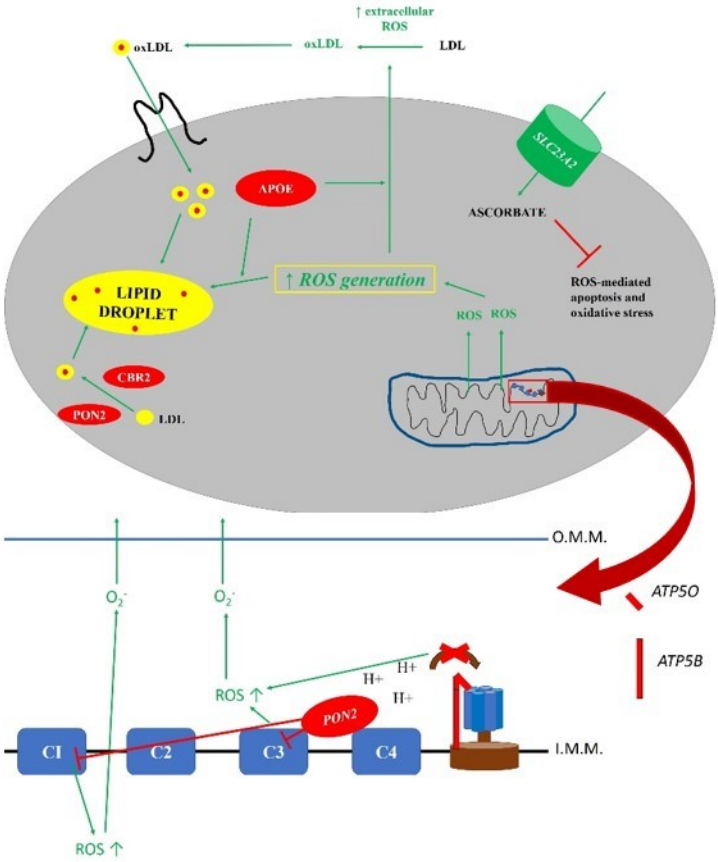

Figure 12. BMDM derived from *Pg* recipient mice display methylation and expression changes consistent with increased oxidative stress and ROS production. *ATP5O, ATP5F1,* and *PON2* hypermethylation and downregulation promotes ETC dysfunction, impaired mitochondrial antioxidant activity, and increased mitochondrial ROS production. Furthermore, hypermethylation of *PON2*, *APOE,* and *CBR2* would promote further cytoplasmic oxidative stress, resulting in production and accumulation of oxLDL. ROS generated and released by *Pg* recipient macrophages, in the sub-intimal environment, containing high levels of LDL could promote generation of oxLDL and promote unregulated uptake, increasing lipid droplet size and oxLDL content. To withstand ROS-mediated intracellular damage, and thus promote oxLDL production, *SLC23A2* hypomethylation and upregulation promotes vitamin C uptake, preventing macrophage apoptosis and oxidative stress, without impairing uptake of oxLDL. Genes identified in red shapes were hypermethylated and downregulated; those in green were hypomethylated and upregulated. Abbreviations: O.M.M – outer mitochondrial membrane; I.M.M – inner mitochondrial membrane.

contributed to by dysfunction of complexes I and III[123]. The impairment of the ETC, as well as the antioxidant capabilities of the mitochondria, represent mechanisms increasing ROS production.

Furthermore, hypermethylation and downregulation of additional genes have implications in ROS accumulation in the lipid droplet (Fig. 12). *CBR2*, encoding carbonyl reductase 2, is a member of a family of enzymes known for preventing lipid peroxidation[124], one of the critical pathways by which oxLDL production occurs in foam cells[125]. *APOE*, encoding apolipoprotein E, has been shown to have a critical role in regulating oxidative stress, with *APOE* KO macrophages displaying elevated ROS production[126,127]. In addition to its mitochondrial function, *PON2* has cytoplasmic anti-oxidant function, with studies showing the role of cytoplasmic *PON2* in preventing intracellular LDL oxidation[125]. Together, not only will increased ROS levels intracellularly lead to oxLDL production, but leakage into the extracellular space has implications for macrophages in the sub-intimal space, with the possibility of increased, non-regulated uptake of oxLDL generated extracellularly (Fig. 12).

Elevated ROS production is often a precursor step to cell apoptosis[128]. For *Pg* recipient macrophages to withstand ROS-mediated intracellular damage, and thus promote oxLDL production necessary for atherosclerosis progression, *SLC23A2*, encoding a sodium-dependent vitamin C transporter, was hypomethylated and upregulated (Table 5). Vitamin C is a key antioxidant that has been suggested in *in vitro* studies to prevent macrophage apoptosis and oxidative stress, without impairing uptake of oxLDL[129]. *In vivo* studies support *SLC23A2*'s key role in promoting atherosclerosis and macrophage survival[130]. Together, the expression and methylation patterns of these six genes suggests a macrophage undergoing oxidative stress. Mitochondrial ROS production promotes oxLDL formation both intracellularly, and extracellularly with its release into intimal spaces. In the presence of increased vitamin C to help

the cell deal with oxidative stress, unregulated oxLDL uptake is amplified with increased extracellular levels, thus increasing oxLDL presence in the lipid droplet.

3.13 BMDM from *Pg* recipient mice display methylation and expression changes consistent with increased triglyceride and cholesterol accumulation

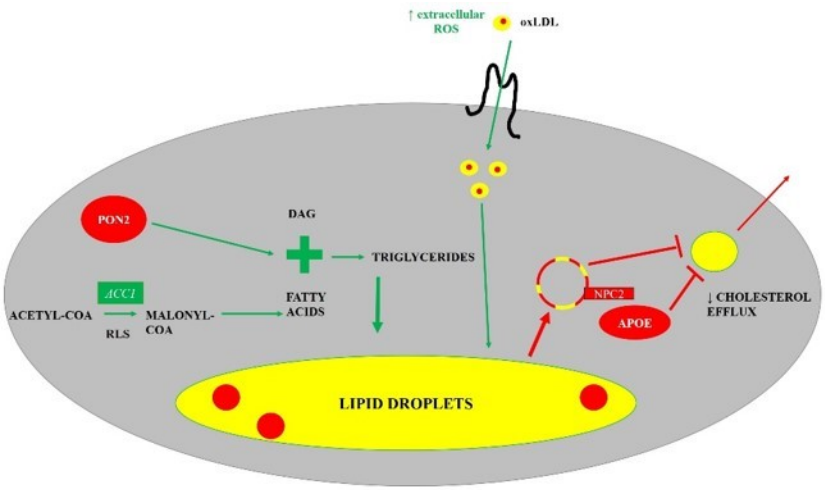

Figure 13. *Pg* recipient macrophages display methylation and expression changes consistent with increased triglyceride and cholesterol accumulation. Hypomethylation of *ACC1*, encoding acetyl-CoA carboxylase 1, promotes fatty acid synthesis, which, in combination with *PON2* hypermethylation and downregulation promotes triglyceride synthesis. Together with increased availability of cholesterol due to ROS-enhanced extracellular LDL and unregulated uptake, triglyceride synthesis would contribute to cytoplasmic lipid accumulation. *APOE* and *NPC2* (encoding NPC intracellular cholesterol transporter 2), both of which were hypermethylated and downregulated, are two proteins important in cholesterol efflux. Genes identified in red shapes were hypermethylated and downregulated; those in green were hypomethylated and upregulated. Abbreviations: RLS: rate limiting step.

In addition to methylation and sequencing data suggesting a more pro-oxidative phenotype, changes were observed in *Pg* recipient mice consistent with increased triglyceride and cholesterol accumulation (shown in Fig. 13), both traits consistent with foam cell formation[131-133]. Intracellular triglyceride and cholesterol are stored as part of an esterified cholesterol droplet, whose size becomes dysregulated in foam cells[134]. Acetyl-CoA carboxylase 1, encoded by *ACC1*, was hypomethylated and upregulated. This enzyme catalyzes the rate limiting step in fatty acid synthesis, converting acetyl-CoA into malonyl CoA[135]. This, in combination with the *PON2* deficiency, which has been shown to increase macrophage triglyceride synthesis and content[136], would promote triglyceride accumulation, and thus lipid droplet size (Fig 12, 13). Furthermore, increased availability of

cholesterol due to ROS-enhanced extracellular oxLDL and unregulated uptake, would contribute to a greater lipid droplet. As mentioned previously, the size of the lipid droplet in steady state is regulated, with excess esterified cholesterol being transported to the plasma membrane and removed by efflux pathways[25,26]. *APOE* and *NPC2* (encoding NPC intracellular cholesterol transporter 2), both of which were hypermethylated and downregulated, are two important proteins in this process[26,137,138] (Fig.13). A reduction in cholesterol efflux is consistent with the reduced HDL production observed in the plasma (Fig. 7B), as *APOE* is a key mediator in the formation of HDL[39]. Impaired cholesterol efflux, together with increased triglyceride and cholesterol accumulation, suggests an increase in the lipid droplet size.

3.14 *Pg* recipient macrophages display methylation and expression changes consistent with impaired trafficking and catabolism of triglyceride-rich lipoproteins

Once in the plasma, HDL has the ability to exchange *APOE* with VLDL and its intermediates, such as intermediate low-density lipoprotein (IDL), so that it can be cleared by the remnant receptor pathway in the liver[39] (Fig. 14). The lack of exchange, due to hypermethylation and downregulation of macrophage *APOE* may contribute to lack of VLDL and IDL clearance; this is supported in part by the higher VLDL triglyceride fraction in the *Pg* recipients (Fig. 8A), thus leading to increased plasma triglycerides (Fig. 5B). However, macrophage *APOE* in the plasma only accounts for a small proportion (5-10%) of total plasma *APOE*[139], thus this may only represent a minor mechanism. Another gene, which was upregulated and hypomethylated in *Pg* recipient macrophages was *SORL1* (sortilin-related receptor 1). This protein has been shown to prevent triglyceride liberation from plasma VLDL through two major mechanisms[140], regulating

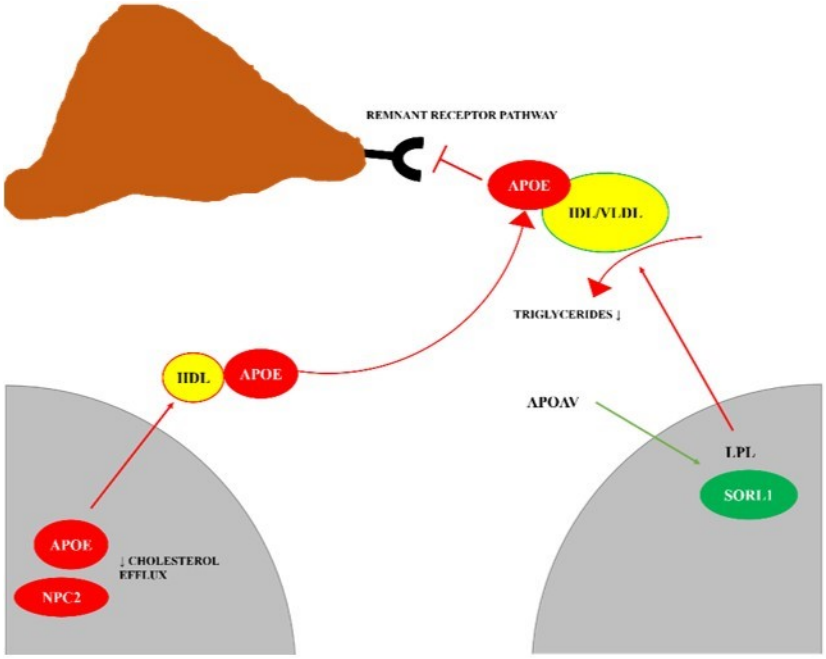

Figure 14. Genes involved in plasma catabolism and trafficking of lipids are differentially methylated and regulated in *Pg* recipient mice. Once in the plasma, HDL can exchange *APOE* with VLDL and its remnants, such as intermediate low-density lipoprotein (IDL), for liver clearance by the remnant receptor pathway in the liver. Hypermethylation and downregulation of macrophage *APOE* may contribute to lack of VLDL and IDL clearance. Hypomethylation and upregulation of *SORL1*, which has been shown to regulate cellular lipoprotein lipase secretion and uptake of its apoAV activator, would prevent triglyceride hydrolysis of VLDL. Genes identified in red shapes were hypermethylated and downregulated; those in green were hypomethylated and upregulated.

lipoprotein lipase secretion and uptake of apoAV, a lipase plasma activator[141,142] (Fig. 14). Thus, the combination of *APOE* downregulation and *SORL1* upregulation could provide a mechanistic basis by which the plasma triglycerides (Fig. 5B) and esterified cholesterol (Fig. 6B) in the *Pg* recipients are elevated. Generally, foam cells are associated with increased triglyceride uptake from their surrounding environment[143], however it may be that the increase in intracellular synthesis is the major contributive factor to the foam cell phenotype in *Pg* recipients (Fig. 13). This leaves high plasma triglycerides as a potential pro-atherogenic mechanism for other cell types involved in atherosclerosis including endothelial cells, promoting dysfunction[144,145] that may accelerate atherosclerosis development.

CHAPTER 4

General Discussion

The objective of the studies outlined in this dissertation was to catalog DNA methylation changes in the bone marrow of *Pg*-infected mice, and use data mining, transcriptome analysis, and systemic lipid analysis to identify changes in immune cell gene methylation consistent with a pro-atherogenic phenotype. These experiments were performed as a model of periodontitis-induced persistence of CVD risk, whereby transplant of bone marrow from orally-infected *Pg* donors into naïve recipients allowed *Pg*-induced bone marrow changes to be present in recipients without direct effects of elevated *Pg.* While oral *Pg* infection in mice is one of the most extensively used mouse models of periodontitis[102-105], it does suffer some limitations in its applicability to periodontitis in humans. Periodontitis is more complex than infection by one periodontal pathogen; it is characterized by a response to a diverse bacterial biofilm in a susceptible (either genetically or medically) host, foundational traits not replicated in this mouse model[46,146]. Thus, any conclusions based on these studies need to be placed in the context of a *Pg* infection, as a model, rather than true representation of periodontitis in humans.

WGBS and mRNA-seq studies allowed a global approach to identifying genes differentially methylated and transcribed, promoting a pro-atherogenic phenotype in immune cells. Rather than isolating HSC hypothesized as the vehicle for propagating changes in DNA methylation long-term, immediate downstream bone marrow progenitors were used as a surrogate owing to the limited size of the HSC population[98] and the feasibility of collecting enough DNA for sequencing. In our studies, each replicate was only sequenced at a coverage of around 10x; a coverage of 20x per replicate is recommended by the NIH Roadmap Epigenomics Project to gauge whole genome methylation[147], but this continues to evolve. This sparser sequencing depth may play a role in why no significant differences in total genome methylation were observed between *Pg* and sham samples (Fig. 9A). Recent studies in patients with diabetes, hypertension, and chronic

kidney disease have shown global leukocyte hypermethylation as a predisposing factor for CVD events[148,149]. This trend to genome hypermethylation has been supported by studies in human atherosclerotic lesions[150]. Thus, repeating these experiments in this mouse model are key at a higher coverage, and are warranted given the skew to promoter hypermethylation observed at the gene level in *Pg* donor bone marrow progenitors (Fig. 9B). However, for identification of DMRs and DMPs, coverage of 5x-10x has been used in other WGBS studies[151,152], and was thus sufficient for analysis at the gene level.

It was necessary to confirm that differential methylation identified by WGBS correlated with changes in transcription, thus mRNA-seq was performed on macrophages derived from the bone marrow of recipient mice. This provided a basis for representing persistence of these epigenetic changes, 8 months post-transplant and without *Pg* challenge. An 8-month endpoint was chosen for these studies to determine if any epigenetic and systemic phenotype changes could be observed at a timepoint longer than the initial 16-20 week endpoint used in preliminary studies in figures 2 and 4. In the experiments following these preliminary studies, ensuring macrophages were derived from bone marrow was key to eliminating the mRNA input of peripheral tissue resident macrophages. However, deriving macrophages from a total bone marrow cell population did not account for contamination with macrophage memory cells homing to the bone marrow. While the macrophage memory response has not been described in response to periodontal pathogens as of yet, the idea of innate immune memory is one that has been shown for a variety of other infections[153-155]. Therefore, future studies are necessitated to derive macrophages from a purer bone marrow progenitor population, such as those used for WGBS, to eliminate these as possible contaminating cells in sequencing experiments.

Following completion of experiments, several genes corresponding to critical macrophage functions in atherosclerosis were enriched in differential methylation and expression. The idea of mitochondrial dysfunction leading to increased ROS production has been suggested as a key mechanism in cardiovascular disease, atherosclerosis and foam cell formation[156-159]. In *Pg* recipient mice, hypermethylation and downregulation in subunits of ATP synthase of the ETC (*ATP5O, ATPF1*) and mitochondrial antioxidant enzymes (*PON2*) represent a mechanistic basis by which macrophages derived from this bone marrow are epigenetically pre-disposed to elevated mitochondrial ROS production (Fig. 12). Downregulation of other subunits of ATP synthase in cardiac disease and increased O_2^- production have been reported recently[120], highlighting the role mitochondrial dysfunction plays in CVD progression. Once in the cytoplasm, mitochondrial ROS may promote lipid droplet oxidation, increasing its oxLDL content, especially as hypermethylation and downregulation of genes involved in cytoplasmic lipid antioxidant activity (*CBR2, PON2*) and ROS production (*APOE*) would prevent cellular pathways responsible for detoxification of oxLDL (Fig. 12). High intracellular oxLDL content represents another key characteristic of foam cells[125,160,161]. Furthermore, extracellular release of this ROS is key not only to promoting oxLDL production in the intimal spaces LDL[18] for further macrophage uptake (Fig. 12), but the uptake of oxLDL by other cell types also promotes atherosclerotic progression. For example, endothelial cells, like macrophages have been shown to express oxLDL receptors[162], and its uptake has been shown to promote expression of leukocyte adhesion molecules[163], intracellular ROS production[164], and cell proliferation[165], all key endothelial functions promoting atherosclerosis. To improve survival in oxidative stress, macrophages from *Pg* recipient mice displayed hypomethylation and upregulation of *SLC23A2,* a vitamin-C transporter shown to be critical in preventing cellular apoptosis during times of oxidative stress[128,130] (Fig 12). This, in combination with pro-oxidative

mitochondrial changes in methylation and expression, suggest a phenotype in *Pg* recipient macrophages consistent with promoting intracellular oxLDL formation, ROS generation, and oxLDL uptake.

The intracellular accumulation of oxLDL in *Pg* recipient mice is further amplified by the increase in the size of the lipid droplet, suggested by triglyceride accumulation (due to synthesis increase by *PON2* deficiency and *ACC1* increase), the increase in oxLDL unregulated uptake, as well as deficiencies in cholesterol efflux (*NPC2, APOE*) (Fig. 13). Deficiencies in cholesterol efflux are consistent with decreased plasma HDL formation in *Pg* recipient mice (Fig. 7B). In human studies, macrophage cholesterol efflux impairment observed in monocytes derived from high-risk patients did not seem to contribute to total plasma HDL[166]. However, it may be important to consider that any epigenetic changes induced in HSC in *Pg*-infected donors can manifest in many other immune cell types, including dendritic cells, in which *APOE* deficiency promoted cholesterol accumulation, antigen presentation and T cell activation[167]. Thus, from a multicellular perspective, impaired cholesterol efflux from many cell types in the immune system may be sufficient to result in the *in vivo* plasma HDL effects observed in these studies.

As part of this dissertation, while no phenotypic analysis was done at the cellular level, there was interest in the possibility of bone marrow-derived epigenetic changes impacting systemic phenotype, specifically plasma lipid phenotype. In addition to the HDL differences observed (Fig. 7B), the analysis of plasma cholesterol and triglycerides, as well as their plasma lipoprotein distribution gleaned three other interesting trends. The first was increased total plasma triglycerides in *Pg* recipient mice (Fig. 5B). This was attributed to the combinatorial effects of *APOE* hypermethylation and downregulation, as well as *SORL1* hypomethylation and upregulation (Fig. 14). Along with the greater esterified cholesterol fraction uncovered in *Pg* recipient mice

(Fig. 6B) and VLDL triglycerides (Fig. 8B), these results may suggest decreased triglyceride catabolism by macrophages (and immune cells from *Pg* bone marrow as a whole). As with the results seen in HDL, the idea that initiation of these epigenetic changes in not only macrophages, but many cells of the immune system from a common stem cell, may provide an explanation as to how these epigenetic changes may manifest systemically.

The differences in methylation and transcriptional expression of genes involved in mitochondrial ROS production[168], increase in cytoplasmic oxLDL[169], fatty acid synthesis[170], and impaired cholesterol efflux[171] are highly suggestive of a more pro-inflammatory M1 macrophage phenotype. M1 macrophages have been shown to be big players in *in vitro*[172], as well as *in vivo Pg* studies measuring alveolar bone loss[173,174]. It is interesting that many of the changes in methylation and mRNA expression observed in *Pg* recipient mice correlated with this macrophage phenotype, suggesting a "memory" effect where the bone marrow is conditioned to respond as if *Pg* is still present.

From a more global perspective, oxidative phosphorylation, oxidative metabolism, and cell detoxification were identified more broadly by GO, KEGG, and Reactome analyses to contain many genes differentially regulated (Tables 3 and 4), many more than the nine genes identified above. This begs the question as to whether there are other epigenetic mechanisms at play outside of DNA methylation. Histone modifications may be induced in *Pg* recipient BMDM that are leading to these differences, as these genes were not identified to be differentially methylated by WGBS. Those of particular interest are histone acetylation[175] and methylation[176], which have been shown to be key regulators of atherosclerosis development, and need to be included as part of the epigenetic analyses in future experiments.

In interpretation of the results as whole, it is important to regard these sequencing studies as observational in nature, identifying candidate pro-atherogenic trends in gene methylation and expression for further phenotypic testing. This is because they lack data validation with qPCR (for mRNA seq), validation at the protein level, and validation of effects on cellular and systemic lipid phenotype. These are experiments that are now being planned and will be performed in the future. Building on these studies, future experiments should have three aims. First, they must validate the mechanistic role of bone marrow DNA methylation, by repeating them in presence of DNA methyltransferase inhibitors, such as 5-aza-2'-deoxycytidine, shown in atherosclerosis studies to reverse methylation changes promoting inflammatory macrophages[90]. Second, studies should be repeated in HFD-fed recipient mice rather than normal chow-fed mice. With atherosclerosis and cardiovascular disease being multifactorial, placing persistent risk due to *Pg* infection in a hypercholesteremic environment induced in the HFD model would allow for the observation of potential synergetic effects of multi risk-factor presence on immune cell methylation, and thus phenotype. Third, while DNA methylation is one of the major epigenetic mechanisms used by cells to control gene expression, epigenetic studies may be expanded to look at histone modifications, especially because a number of differentially methylated genes identified in mRNA-seq could not be correlated to changes in DNA methylation.

In addition to studies needing to validate phenotype, studies evaluating the mechanistic basis by which *Pg* infection imparts epigenetic changes in the bone marrow need to be performed. As mentioned, one of the predominant beliefs as to how periodontitis and CVD are related is through systemic inflammation[59,60]. One aspect of this inflammation is oxidative stress, which has been shown in studies to be increased systemically in periodontitis patients[177-179]. Research into other inflammatory diseases, including diabetes, has shown that oxidative stress induces DNA

methylation changes contributing to diabetic complications including blindness[180], as well as wound healing[181]. In diabetic mouse studies, transplantable changes in DNA methylation observed in HSC were responsible for M1 macrophage polarization and impaired wound healing in bone marrow recipients[181], highlighting the role HSC methylation status may have on persistent disease risk after. Thus, future studies should strive to confirm oxidative stress as the mechanistic basis for these epigenetic changes, using systemic antioxidant treatment in donor mice to ablate pro-atherogenic epigenetic changes induced by *Pg* infections.

These studies were inspired by studies in edentulous patients, which no longer have periodontitis, but have either the same risk as periodontitis patients for CVD or residual long-term risk[66-69]. Unfortunately, studies assessing periodontitis treatment in dentate patients and its effect on CVD risk long-term are lacking, with systematic reviews identifying only very low-level evidence[182]. This is important, when a more representative measure of clinically acceptable periodontitis elimination in the current periodontology climate is non-surgical and surgical options in dentate patients, allowing them to retain their teeth. In a recent article published on the American College of Cardiology Website[183], two key reasons why such studies are difficult to conduct were suggested, owing to the requirements of large sample sizes and ethical considerations of refusing periodontal treatments to a control group. Thus, these reasons need to be kept in mind when planning studies to address whether residual risk remains long-term even with periodontal treatment in dentate patients.

It is key to consider, however that while such studies have not been conducted in periodontitis patients, there have been studies following elimination of other CVD risk factors, and they have supported reduced risk following disease treatment. For example, recent studies in smoking cessation[184] and statin-treated hyperlipidemic patients[185] show reduced CVD risk and

events over a 5 year period, suggesting that risk factor intervention can have beneficial effects in shorter timelines. Therefore, studies with longer follow-up periods, as long as 20 years[74], are key to establishing that residual risk remains long-term, and thus it is key to implement control strategies for other risk factor a patient may present with, such that this residual risk is not the tipping point to suffering a CVD event.

While in the beginning stages, these studies and those in the future will contribute to the idea that epigenetic processes may be responsible for persistent risk. This is a relatively new and paradigm-shifting concept, especially in the field of therapeutics and CVD. These studies will necessitate the development of CVD therapeutics against epigenetic processes, or inflammatory pathways that promote these changes. These ideas may also apply in a broader context, even to other risk factors for CVD; studies in diabetic mice have already shown hyperglycemia-induced inflammation to induce bone marrow-derived epigenetic changes contributing to disease progression and persistence such as diabetes[181,186]. The targeting of epigenetic processes with treatment and pharmacology isn't novel and has been gaining steam in recent years, especially in cancers, where histone deacetylase inhibitors[187] and DNA methylation inhibitors[188] have been tested as potential therapeutic options in the last decade. Epigenetic re-programming of cells in cardiovascular disease, and many others for that matter, represents another frontier in health that is promising, not only in terms of understanding disease pathogenesis, but also providing each patient with an individualized approach of treatment specific to their epigenetic background.

References

1. Roth GA, Abate D, Abate KH, Abay SM, Abbafati C, Abbasi N, et al. Global, regional, and national age-sex-specific mortality for 282 causes of death in 195 countries and territories, 1980–2017: A systematic analysis for the global burden of disease study 2017. The Lancet 2018; 392(10159):1736-1788.

2. The Public Health Agency in Canada. The Economic Burden of Illness in Canada, 2010. 2017; Available from: https://www.canada.ca/en/public-health/services/publications/science-research-data/economic-burden-illness-canada-2010.html#cost. [cited June 20, 2020].

3. Leal J, Luengo-Fernández R, Gray A, Petersen S, Rayner M. Economic burden of Cardiovascular Diseases in the Enlarged European Union. Eur Heart J 2006; 27(13): 1610-1619.

4. Mendis S, Lindholm LH, Mancia G, Whitworth J, Alderman M, Lim S, et al. World Health Organization (WHO) and International Society of Hypertension (ISH) Risk Prediction Charts: Assessment of Cardiovascular Risk for Prevention and Control of Cardiovascular Disease in Low and Middle-Income Countries. J Hypertens 2007; 25(8):1578-1582.

5. Mahmood SS, Levy D, Vasan RS, Wang TJ. The Framingham Heart Study and the Epidemiology of Cardiovascular Disease: A Historical Perspective. The Lancet 2014; 383(9921): 999-1008.

6. Framingham Heart Study: Three Generations of Dedication. Epidemiological Background and Design: The Framingham Heart Study. Available from: https://framinghamheartstudy.org/fhs-about/history/epidemiological-background/. [cited May 1, 2020].

7. Castelli WP, Garrison RJ, Wilson PWF, Abbott RD, Kalousdian S, Kannel WB. Incidence of Coronary Heart Disease and Lipoprotein Cholesterol Levels: The Framingham Study. JAMA 1986; 256(20): 2835-2838.

8. Stamler J, Wentworth D, Neaton JD. Is Relationship Between Serum Cholesterol and Risk of Premature Death From Coronary Heart Disease Continuous and Graded?: Findings in 356 222 Primary Screenees of the Multiple Risk Factor Intervention Trial (MRFIT). JAMA 1986; 256(20): 2823-2828.

9. Castelli WP. The triglyceride issue: A view from Framingham. American Heart Journal 1986; 112(2): 432-437.

10. Sarwar N, Danesh J, Eiriksdottir G, Sigurdsson G, Wareham N, Bingham S, et al. Triglycerides and the Risk of Coronary Heart Disease. Circulation 2007; 115(4): 450-458.

11. Kannel WB, McGee DL. Diabetes and Cardiovascular Disease: The Framingham Study. JAMA 1979; 241(19): 2035-2038.

12. Freund KM, Belanger AJ, D'Agostino RB, Kannel WB. The health risks of smoking the framingham study: 34 years of follow-up. Annals of Epidemiology 1993; 3(4): 417-424.

13. Dikalov S, Itani H, Richmond B, Arslanbaeva L, Vergeade A, Rahman SMJ, et al. Tobacco Smoking Induces Cardiovascular Mitochondrial Oxidative Stress, Promotes Endothelial Dysfunction, and Enhances Hypertension. American Journal of Physiology - Heart and Circulatory Physiology 2019; 316(3): H639-H646.

14. Ross R. The Pathogenesis of Atherosclerosis — an update. N Engl J Med 1986; 314(8): 488-500.

15. Lerman A, Burnett Jr JC. Intact and Altered Endothelium in Regulation of Vasomotion. Circulation 1992; 86(6): III12-III19.

16. Hadi HAR, Carr CS, Al Suwaidi J. Endothelial Dysfunction: Cardiovascular Risk Factors, Therapy, and Outcome. Vascular Health and Risk Management 2005; 1(3): 183-198.

17. Su JB. Vascular Endothelial Dysfunction and Pharmacological Treatment. World Journal of Cardiology 2015; 7(11): 719-741.

18. Ira T, Williams KJ, Borén J. Subendothelial Lipoprotein Retention as the Initiating Process in Atherosclerosis. Circulation 2007; 116(16): 1832-1844.

19. Williams KJ. Arterial wall chondroitin sulfate proteoglycans: Diverse molecules with distinct roles in lipoprotein retention and atherogenesis. Curr Opin Lipidol 2001;12(5): 477-487.

20. Stary HC, Chandler AB, Glagov S, Guyton JR, Insull W, Rosenfeld ME, et al. A definition of initial, fatty streak, and intermediate lesions of atherosclerosis. A report from the Committee on Vascular Lesions of the Council on Arteriosclerosis, American Heart Association. Circulation 1994; 89(5): 2462-2478.

21. Mead JR, Irvine SA, Ramji DP. Lipoprotein lipase: structure, function, regulation, and role in disease. Journal of Molecular Medicine 2002; 80(12): 753-769.

22. Patel Kevin M, Alanna S, Junichiro T, Xueting J, Morales Carlos R, Jeffery B, et al. Macrophage Sortilin Promotes LDL Uptake, Foam Cell Formation, and Atherosclerosis. Circ Res 2015; 116(5): 789-796.

23. Hoff HF, O'Neil J, Pepin JM, Cole TB. Macrophage uptake of cholesterol-containing particles derived from LDL and isolated from atherosclerotic lesions. Eur Heart J 1990; 11(suppl_E): 105-115.

24. Zhang L, Reue K, Fong LG, Young SG, Tontonoz P. Feedback Regulation of Cholesterol Uptake by the LXR–IDOL–LDLR Axis. Arterioscler Thromb Vasc Biol 2012; 32(11): 2541-2546.

25. Wang X, Collins HL, Ranalletta M, Fuki IV, Billheimer JT, Rothblat GH, et al. Macrophage ABCA1 and ABCG1, but not SR-BI, promote macrophage reverse cholesterol transport in vivo. J Clin Invest 2007; 117(8): 2216-2224.

26. Zanotti I, Pedrelli M, Potì F, Stomeo G, Gomaraschi M, Calabresi L, et al. Macrophage, But Not Systemic, Apolipoprotein E Is Necessary for Macrophage Reverse Cholesterol Transport In Vivo. Arterioscler Thromb Vasc Biol 2011; 31(1): 74-80.

27. Miller NE. HDL metabolism and its role in lipid transport. Eur Heart J 1990; 11(suppl_H): 1-3.

28. Lin H, Lii C, Chen H, Lin A, Yang Y, Chen H. Andrographolide inhibits oxidized LDL-induced cholesterol accumulation and foam cell formation in macrophages. Am J Chin Med 2018; 46(1): 87-106.

29. Goldstein JL, Ho YK, Basu SK, Brown MS. Binding site on macrophages that mediates uptake and degradation of acetylated low density lipoprotein, producing massive cholesterol deposition. Proc Natl Acad Sci U S A 1979; 76(1): 333-337.

30. Chistiakov DA, Bobryshev YV, Orekhov AN. Macrophage-mediated cholesterol handling in atherosclerosis. J Cell Mol Med 2016; 20(1):17-28.

31. Fan LM, Douglas G, Bendall JK, McNeill E, Crabtree MJ, Hale AB, et al. Endothelial Cell-Specific Reactive Oxygen Species Production Increases Susceptibility to Aortic Dissection. Circulation 2014; 129(25): 2661-2672.

32. Wang Y, Wang GZ, Rabinovitch PS, Tabas I. Macrophage Mitochondrial Oxidative Stress Promotes Atherosclerosis and Nuclear Factor-κB–Mediated Inflammation in Macrophages. Circ Res 2014; 114(3): 421-433.

33. Berenson GS, Srinivasan SR, Bao W, Newman WP, Tracy RE, Wattigney WA. Association Between Multiple Cardiovascular Risk Factors and Atherosclerosis in Children and Young Adults. N Engl J Med 1998; 338(23): 1650-1656.

34. Murat TE, Kapadia Samir R, Eralp T, Ziada Khaled M, Hobbs Robert E, McCarthy Patrick M, et al. High Prevalence of Coronary Atherosclerosis in Asymptomatic Teenagers and Young Adults. Circulation 2001; 103(22): 2705-2710.

35. Xie J, Wang J, Tang T, Chen J, Gao X, Yuan J, et al. The Th17/treg functional imbalance during atherogenesis in ApoE−/− mice. Cytokine 2010; 49(2): 185-193.

36. Tay C, Kanellakis P, Hosseini H, Cao A, Toh B, Bobik A, et al. B cell and CD4 T cell interactions promote development of atherosclerosis. Frontiers in Immunology 2020; 10: 3046.

37. Alexander MR, Owens GK. Epigenetic Control of Smooth Muscle Cell Differentiation and Phenotypic Switching in Vascular Development and Disease. Annu Rev Physiol 2012; 74(1): 13-40.

38. Labropoulos N, Zarge J, Mansour MA, Kang SS, Baker WH. Compensatory arterial enlargement is a common pathobiologic response in early atherosclerosis. The American Journal of Surgery 1998; 176(2): 140-143.

39. Linton MF, Yancey PG, Davies SS, Jerome WG, Linton EF, Song WL, et al. The Role of Lipids and Lipoproteins in Atherosclerosis. In: Feingold KR, Anawalt B, Boyce A, Chrousos G, Dungan K, Grossman A, et al, editors. Endotext South Dartmouth (MA): MDText.com, Inc.; 2000.

40. Lockhart PB, Bolger AF, Papapanou PN, Osinbowale O, Trevisan M, Levison ME, et al. Periodontal Disease and Atherosclerotic Vascular Disease: Does the Evidence Support an Independent Association?: A Scientific Statement From the American Heart Association. Circulation 2012 May 22; 125(20): 2520-2544.

41. Sen S, Sumner R, Hardin J, Barros S, Moss K, Beck J, et al. Periodontal Disease and Recurrent Vascular Events in Stroke/Transient Ischemic Attack Patients. Journal of Stroke and Cerebrovascular Diseases 2013; 22(8): 1420-1427.

42. Johansson CS, Richter A, Lundström Å, Thorstensson H, Ravald N. Periodontal conditions in patients with coronary heart disease: A case–control study. J Clin Periodontol 2008; 35(3): 199-205.

43. Beck JD, Elter JR, Heiss G, Couper D, Mauriello SM, Offenbacher S. Relationship of Periodontal Disease to Carotid Artery Intima-Media Wall Thickness. Arterioscler Thromb Vasc Biol 2001; 21(11): 1816-1822.

44. Könönen E, Gursoy M, Gursoy UK. Periodontitis: A Multifaceted Disease of Tooth-Supporting Tissues. Journal of Clinical Medicine 2019; 8(8): 1135.

45. Khan SA, Kong EF, Meiller TF, Jabra-Rizk M. Periodontal Diseases: Bug Induced, Host Promoted. PLoS Pathogens 2015; 11(7): e1004952.

46. Colombo APV, Boches SK, Cotton SL, Goodson JM, Kent R, Haffajee AD, et al. Comparisons of Subgingival Microbial Profiles of Refractory Periodontitis, Severe Periodontitis, and Periodontal Health Using the Human Oral Microbe Identification Microarray. J Periodontol 2009; 80(9): 1421-1432.

47. Suzuki N, Yoneda M, Hirofuji T. Mixed Red-Complex Bacterial Infection in Periodontitis. International Journal of Dentistry 2013; 2013: 587279.

48. Hendrickson EL, Xia Q, Wang T, Lamont RJ, Hackett M. Pathway analysis for intracellular *Porphyromonas gingivalis* using a strain ATCC 33277 specific database. BMC Microbiology 2009; 9: 185.

49. Tan KH, Seers CA, Dashper SG, Mitchell HL, Pyke JS, Meuric V, et al. *Porphyromonas gingivalis* and *Treponema denticola* Exhibit Metabolic Symbioses. PLoS Pathogens 2014; 10(3): e1003955.

50. Castro SA, Collighan R, Lambert PA, Dias IHK, Chauhan P, Bland CE, et al. *Porphyromonas gingivalis* gingipains cause defective macrophage migration towards apoptotic cells and inhibit phagocytosis of primary apoptotic neutrophils. Cell Death & Disease 2017; 8(3): e2644.

51. Chen T, Nakayama K, Belliveau L, Duncan MJ. *Porphyromonas gingivalis* gingipains and adhesion to epithelial cells. Infect Immun 2001; 69(5): 3048-3056.

52. Mydel P, Takahashi Y, Yumoto H, Sztukowska M, Kubica M, Gibson FC, et al. Roles of the host oxidative immune response and bacterial antioxidant rubrerythrin during *Porphyromonas gingivalis* infection. PLoS Pathogens 2006; 2(7): e76.

53. Slaney JM, Gallagher A, Aduse-Opoku J, Pell K, Curtis MA. Mechanisms of Resistance of *Porphyromonas gingivalis* to Killing by Serum Complement. Infect Immun 2006; 74(9): 5352-5361.

54. Hajishengallis G, Lamont RJ. Beyond the red complex and into more complexity: The polymicrobial synergy and dysbiosis (PSD) model of periodontal disease etiology. Molecular Oral Microbiology 2012; 27(6): 409-419.

55. Armitage GC. Development of a Classification System for Periodontal Diseases and Conditions. Annals of Periodontology 1999; 4(1): 1-6.

56. Armitage GC, Cullinan MP. Comparison of the clinical features of chronic and aggressive periodontitis. Periodontol 2000 2010; 53(1): 12-27.

57. Caton JG, Armitage G, Berglundh T, Chapple ILC, Jepsen S, Kornman KS, et al. A new classification scheme for periodontal and peri-implant diseases and conditions – Introduction and key changes from the 1999 classification. J Clin Periodontol 2018; 45(suppl_20): S1-S8.

58. Tonetti MS, Greenwell H, Kornman KS. Staging and grading of periodontitis: Framework and proposal of a new classification and case definition. J Periodontol 2018; 89(suppl_1): S159-S172.

59. Brown PM, Kennedy DJ, Morton RE, Febbraio M. CD36/SR-B2-TLR2 Dependent Pathways Enhance *Porphyromonas gingivalis* Mediated Atherosclerosis in the Ldlr KO Mouse Model. PLoS One 2015; 10(5): e0125126.

60. Chun YP, Chun KJ, Olguin D, Wang H. Biological foundation for periodontitis as a potential risk factor for atherosclerosis. J Periodont Res 2005; 40(1): 87-95.

61. Liu Z, Liu Y, Song Y, Zhang X, Wang S, Wang Z. Systemic Oxidative Stress Biomarkers in Chronic Periodontitis: A Meta-Analysis. Dis Markers 2014; 2014: 931083.

62. Loos BG, Craandijk J, Hoek FJ, Wertheim-van Dillen PM, van der Velden U. Elevation of systemic markers related to cardiovascular diseases in the peripheral blood of periodontitis patients. J Periodontol 2000; 71(10): 1528-1534.

63. Bermudez EA, Rifai N, Buring J, Manson JE, Ridker PM. Interrelationships Among Circulating Interleukin-6, C-Reactive Protein, and Traditional Cardiovascular Risk Factors in Women. Arterioscler Thromb Vasc Biol 2002; 22(10): 1668-1673.

64. Keaney Jr JF, Larson MG, Vasan RS, Wilson PWF, Lipinska I, Corey D, et al. Obesity and Systemic Oxidative Stress: Clinical Correlates of Oxidative Stress in the Framingham Study. Arterioscler Thromb Vasc Biol 2003; 23(3): 434-439.

65. Haraszthy VI, Zambon JJ, Trevisan M, Zeid M, Genco RJ. Identification of Periodontal Pathogens in Atheromatous Plaques. J Periodontol 2000; 71(10): 1554-1560.

66. Hujoel PP, Drangsholt M, Spiekerman C, Derouen TA. Examining the link between coronary heart disease and the elimination of chronic dental infections. The Journal of the American Dental Association 2001; 132(7): 883-889.

67. Wu T, Trevisan M, Genco RJ, Dorn JP, Falkner KL, Sempos CT. Periodontal Disease and Risk of Cerebrovascular Disease: The First National Health and Nutrition Examination Survey and Its Follow-up Study. Arch Intern Med 2000; 160(18): 2749-2755.

68. DeStefano F, Anda RF, Kahn HS, Williamson DF, Russell CM. Dental disease and risk of coronary heart disease and mortality. BMJ 1993; 306(6879): 688-691.

69. Dietrich T, Jimenez M, Krall Kaye EA, Vokonas PS, Garcia RI. Age-Dependent Associations Between Chronic Periodontitis/Edentulism and Risk of Coronary Heart Disease. Circulation 2008; 117(13): 1668-1674.

70. Talukder MAH, Johnson WM, Varadharaj S, Lian J, Kearns PN, El-Mahdy MA, et al. Chronic cigarette smoking causes hypertension, increased oxidative stress, impaired NO bioavailability, endothelial dysfunction, and cardiac remodeling in mice. American Journal of Physiology - Heart and Circulatory Physiology 2011; 300(1): H388-H396.

71. Morrow JD, Frei B, Longmire AW, Gaziano JM, Lynch SM, Shyr Y, et al. Increase in circulating products of lipid peroxidation (F2-isoprostanes) in smokers — smoking as a cause of oxidative damage. N Engl J Med 1995; 332(18): 1198-1203.

72. Craig WY, Palomaki GE, Haddow JE. Cigarette smoking and serum lipid and lipoprotein concentrations: an analysis of published data. Br Med J 1989; 298(6676): 784-788.

73. Barbieri SS, Zacchi E, Amadio P, Gianellini S, Mussoni L, Weksler BB, et al. Cytokines present in smokers' serum interact with smoke components to enhance endothelial dysfunction. Cardiovasc Res 2011; 90(3): 475-483.

74. Cook DG, Pocock SJ, Shaper AG, Kussick SJ. GIVING UP SMOKING AND THE RISK OF HEART ATTACKS: A report from the British Regional Heart Study. The Lancet 1986; 328(8520): 1376-80.

75. Festa A, D'Agostino R, Howard G, Mykkänen L, Tracy RP, Haffner SM. Chronic Subclinical Inflammation as Part of the Insulin Resistance Syndrome. Circulation 2000; 102(1): 42-47.

76. Kim J, Koh KK, Quon MJ. The Union of Vascular and Metabolic Actions of Insulin in Sickness and in Health. Arterioscler Thromb Vasc Biol 2005; 25(5): 889-891.

77. Napoli C, Triggiani M, Palumbo G, Condorelli M, Chiariello M, Ambrosio G. Glycosylation enhances oxygen radical-induced modifications and decreases acetylhydrolase activity of human low density lipoprotein. Basic Res Cardiol 1997; 92(2): 96-105.

78. Farbstein D, Levy AP. HDL dysfunction in diabetes: Causes and possible treatments. Expert Review of Cardiovascular Therapy 2012; 10(3): 353-361.

79. Nathan DM, Lachin J, Cleary P, Orchard T, Brillon DJ, Backlund JY, O'Leary DH, Genuth S, Diabetes Control and Complications Trial, Epidemiology of Diabetes Interventions and Complications Research Group. Intensive Diabetes Therapy and Carotid Intima–Media Thickness in Type 1 Diabetes Mellitus. N Engl J Med 2003; 348(23): 2294-2303.

80. Nathan DM, Lachin J, Cleary P, Orchard T, Brillon DJ, Backlund JY, O'Leary DH, Genuth S, Diabetes Control and Complications Trial, Epidemiology of Diabetes Interventions and Complications Research Group. Intensive Diabetes Treatment and Cardiovascular Disease In Patients with Type 1 Diabetes. N Engl J Med 2005; 353(25): 2643-2653.

81. Choy JS, Wei S, Lee JY, Tan S, Chu S, Lee T. DNA methylation Increases Nucleosome Compaction and Rigidity. J Am Chem Soc 2010; 132(6): 1782-1783.

82. Yin Y, Morgunova E, Jolma A, Kaasinen E, Sahu B, Khund-Sayeed S, et al. Impact of cytosine methylation on DNA binding specificities of human transcription factors. Science 2017; 356(6337): eaaj2239.

83. Patra SK, Patra A, Zhao H, Dahiya R. DNA methyltransferase and demethylase in human prostate cancer. Mol Carcinog 2002; 33(3): 163-171.

84. Weinhold B. Epigenetics: The Science of Change. Environ Health Perspect 2006; 114(3): A160-A167.

85. Hedrich CM, Crispin JC, Tsokos GC. Epigenetic regulation of cytokine expression in systemic lupus erythematosus with special focus on T cells. Autoimmunity 2014; 47(4): 234-241.

86. Ballestar E. Epigenetic alterations in autoimmune rheumatic diseases. Nat Rev Rheumatol 2011; 7(5): 263-271.

87. van Kampen E, Jaminon A, van Berkel TJC, Van Eck M. Diet-induced (epigenetic) changes in bone marrow augment atherosclerosis. Journal of Leukocyte Biology 2014; 96(5): 833-841.

88. Chen K, Liao Y, Wang J, Lin Y, Chen C, Juo SH. Oxidized low-density lipoprotein is a common risk factor for cardiovascular diseases and gastroenterological cancers via epigenomical regulation of microRNA-210. Oncotarget 2015; 6(27): 24105-24118.

89. Fernández-Sanlés A, Sayols-Baixeras S, Subirana I, Degano IR, Elosua R. Association between DNA methylation and coronary heart disease or other atherosclerotic events: A systematic review. Atherosclerosis 2017; 263: 325-333.

90. Cao Q, Wang X, Jia L, Mondal AK, Diallo A, Hawkins GA, et al. Inhibiting DNA Methylation by 5-Aza-2′-deoxycytidine Ameliorates Atherosclerosis Through Suppressing Macrophage Inflammation. Endocrinology 2014; 155(12): 4925-4938.

91. Ishida K, Kobayashi T, Ito S, Komatsu Y, Yokoyama T, Okada M, et al. Interleukin-6 Gene Promoter Methylation in Rheumatoid Arthritis and Chronic Periodontitis. J Periodontol 2012; 83(7): 917-925.

92. Zhang S, Barros SP, Moretti AJ, Yu N, Zhou J, Preisser JS, et al. Epigenetic Regulation of *TNFA* Expression in Periodontal Disease. J Periodontol 2013; 84(11): 1606-1616.

93. Zhang S, Crivello A, Offenbacher S, Moretti A, Paquette DW, Barros SP. Interferon-gamma promoter hypomethylation and increased expression in chronic periodontitis. J Clin Periodontol 2010; 37(11): 953-961.

94. Benakanakere M, Abdolhosseini M, Hosur K, Finoti LS, Kinane DF. TLR2 Promoter Hypermethylation Creates Innate Immune Dysbiosis. Journal of Dental Research 2015; 94(1): 183-191.

95. Asa'ad F, Bollati V, Pagni G, Castilho RM, Rossi E, Pomingi F, et al. Evaluation of DNA methylation of inflammatory genes following treatment of chronic periodontitis: A pilot case-control study. J Clin Periodontol 2017; 44(9): 905-914.

96. Westera L, Drylewicz J, den Braber I, Mugwagwa T, van der Maas I, Kwast L, et al. Closing the gap between T-cell life span estimates from stable isotope-labeling studies in mice and humans. Blood 2013; 122(13): 2205-2212.

97. Yona S, Kim K, Wolf Y, Mildner A, Varol D, Breker M, et al. Fate Mapping Reveals Origins and Dynamics of Monocytes and Tissue Macrophages under Homeostasis. Immunity 2013; 38(1): 79-91.

98. Seita J, Weissman IL. Hematopoietic Stem Cell: Self-renewal versus Differentiation. Wiley Interdiscip Rev Syst Biol Med 2010; 2(6): 640-653.

99. Trerotola M, Relli V, Simeone P, Alberti S. Epigenetic inheritance and the missing heritability. Human genomics 2015; 9(1): 17.

100. Huszar D, Varban ML, Rinninger F, Feeley R, Arai T, Fairchild-Huntress V, et al. Increased LDL Cholesterol and Atherosclerosis in LDL Receptor-Deficient Mice With Attenuated Expression of Scavenger Receptor B1. Arterioscler Thromb Vasc Biol 2000; 20(4): 1068-1073.

101. Basso F, Amar MJ, Wagner EM, Vaisman B, Paigen B, Santamarina-Fojo S, et al. Enhanced ABCG1 expression increases atherosclerosis in LDLr-KO mice on a western diet. Biochemical and Biophysical Research Communications 2006; 351(2): 398-404.

102. Adamowicz K, Wang H, Jotwani R, Zeller I, Potempa J, Scott DA. Inhibition of GSK3 Abolishes Bacterial-Induced Periodontal Bone Loss in Mice. Mol Med 2012; 18(1): 1190-1196.

103. Hayashi C, Madrigal AG, Liu X, Ukai T, Goswami S, Gudino CV, et al. Pathogen-Mediated Inflammatory Atherosclerosis is Mediated in Part via Toll-Like Receptor 2-Induced Inflammatory Responses. J Innate Immun 2010; 2(4): 334-343.

104. Yang J, Wu J, Zhang R, Yao M, Liu Y, Miao L, et al. *Porphyromonas gingivalis* oral infection promote T helper 17/Treg imbalance in the development of atherosclerosis. Journal of Dental Sciences 2017; 12(1): 60-69.

105. Lalla E, Lamster IB, Hofmann MA, Loredana B, Jerud AP, Tucker S, et al. Oral infection With a Periodontal Pathogen Accelerates Early Atherosclerosis in Apolipoprotein E–Null Mice. Arterioscler Thromb Vasc Biol 2003; 23(8): 1405-1411.

106. Rebel VI, Dragowska W, Eaves CJ, Humphries RK, Lansdorp PM. Amplification of Sca-1+ Lin-WGA+ cells in serum-free cultures containing steel factor, interleukin-6, and erythropoietin with maintenance of cells with long-term in vivo reconstituting potential. Blood 1994; 83(1): 128-136.

107. Krueger F, Andrews SR. Bismark: A flexible aligner and methylation caller for Bisulfite-Seq applications. Bioinformatics 2011; 27(11): 1571-1572.

108. Marim FM, Silveira TN, Lima Jr DS, Zamboni DS. A Method for Generation of Bone Marrow-Derived Macrophages from Cryopreserved Mouse Bone Marrow Cells. PLoS One 2010; 5(12): e15263.

109. Vogel DYS, Heijnen PDAM., Breur M, de Vries HE, Tool ATJ, Amor S, et al. Macrophages migrate in an activation-dependent manner to chemokines involved in neuroinflammation. Journal of Neuroinflammation 2014; 11(1): 23.

110. Rabinovitch M, DeStefano MJ. Use of the local anesthetic lidocaine for cell harvesting and subcultivation. In Vitro 1975; 11(6): 379-381.

111. Han S, Flattery AM, McLaren D, Raubertas R, Lee SH, Mendoza V, et al. Comparison of Lipoprotein Separation and Lipid Analysis Methodologies for Human and Cynomolgus Monkey Plasma Samples. Journal of Cardiovascular Translational Research 2012; 5(1): 75-83.

112. März W, Siekmeier R, Scharnagl H, Seiffert UB, Gross W. Fast lipoprotein chromatography: New method of analysis for plasma lipoproteins. Clin Chem 1993; 39(11): 2276-2281.

113. Ooi BK, Goh BH, Yap WH. Oxidative Stress in Cardiovascular Diseases: Involvement of Nrf2 Antioxidant Redox Signaling in Macrophage Foam Cell Formation. Int J Mol Sci 2017; 18(11): 2336.

114. Gleissner CA, Leitinger N, Ley K. Effects of Native and Modified Low-Density Lipoproteins on Monocyte Recruitment in Atherosclerosis. Hypertension 2007; 50(2): 276-283.

115. Maziere C, Auclair M, Djavaheri-Mergny M, Packer L, Maziere J. Oxidized low density lipoprotein induces activation of the transcription factor NFκB in fibroblasts, endothelial and smooth muscle cells. IUBMB Life 1996; 39(6): 1201-1207.

116. Wang Y, Wang GZ, Rabinovitch PS, Tabas I. Macrophage mitochondrial oxidative stress promotes atherosclerosis and nuclear factor-Kb-mediated inflammation in macrophages. Circ Res 2014; 114: 421-433.

117. Chen H, Morris MA, Rossier C, Blouin J, Antonarakis SE. Cloning of the cDNA for the Human ATP Synthase OSCP subunit (ATP5O) by Exon Trapping and Mapping to Chromosome 21q22.1-q22.2. Genomics 1995; 28(3): 470-476.

118. Higuti T, Tsurumi C, Osaka F, Kawamura Y, Tsujita H, Yoshihara Y, et al. Molecular cloning of cDNA for the import precursor of human subunit B of H(+)-ATP synthase in mitochondria. Biochem Biophys Res Commun 1991; 178(3): 1014-1020.

119. He J, Ford HC, Carroll J, Corsten D, Gonzales E, Ding S, et al. Assembly of the membrane domain of ATP synthase in human mitochondria. Proc Natl Acad Sci USA 2018; 115(12): 2988-2993.

120. Ni R, Zheng D, Xiong S, Hill DJ, Sun T, Gardiner RB, et al. Mitochondrial Calpain-1 Disrupts ATP Synthase and Induces Superoxide Generation in Type 1 Diabetic Hearts: A Novel Mechanism Contributing to Diabetic Cardiomyopathy. Diabetes 2016; 65(1): 255-268.

121. Martínez-Reyes I, Cuezva JM. The H+-ATP synthase: A gate to ROS-mediated cell death or cell survival. Biochim Biophys Acta 2014; 1837(7): 1099-1112.

122. Turrens JF. Mitochondrial formation of reactive oxygen species. J Physiol 2003; 552(Pt 2): 335-344.

123. Devarajan A, Bourquard N, Hama S, Navab M, Grijalva VR, Morvardi S, et al. Paraoxonase 2 Deficiency Alters Mitochondrial Function and Exacerbates the Development of Atherosclerosis. Antioxid Redox Signal 2011; 14(3): 341-351.

124. Ellis EM. Reactive carbonyls and oxidative stress: Potential for therapeutic intervention. Pharmacol Ther 2007; 115(1): 13-24.

125. Ng CJ, Wadleigh DJ, Gangopadhyay A, Hama S, Grijalva VR, Navab M, et al. Paraoxonase-2 is a Ubiquitously Expressed Protein with Antioxidant Properties and is Capable of Preventing Cell-Mediated Oxidative Modification of Low Density Lipoprotein. J Biol Chem 2001; 276(48): 44444-44449.

126. Maor I, Kaplan M, Hayek T, Vaya J, Hoffman A, Aviram M. Oxidized Monocyte-Derived Macrophages in Aortic Atherosclerotic Lesion from Apolipoprotein E-Deficient Mice and from Human Carotid Artery Contain Lipid Peroxides and Oxysterols. Biochem Biophys Res Commun 2000; 269(3): 775-780.

127. R Rosenblat M, Aviram M. Oxysterol-induced activation of macrophage NADPH-oxidase enhances cell-mediated oxidation of LDL in the atherosclerotic apolipoprotein E deficient mouse: inhibitory role for vitamin E. Atherosclerosis 2002; 160(1): 69-80.

128. Virág L, Jaén RI, Regdon Z, Boscá L, Prieto P. Self-defense of macrophages against oxidative injury: Fighting for their own survival. Redox Biology 2019; 26: 101261.

129. Chi X, May JM. Oxidized lipoprotein induces the macrophage ascorbate transporter (SVCT2): protection by intracellular ascorbate against oxidant stress and apoptosis. Arch Biochem Biophys 2009; 485(2): 174-182.

130. Babaev VR, Whitesell RR, Li L, Linton MF, Fazio S, May JM. Selective Macrophage Ascorbate Deficiency Suppresses Early Atherosclerosis. Free Radic Biol Med 2011; 50(1): 27-36.

131. Boström P, Magnusson B, Svensson PA, Wiklund O, Borén J, Carlsson LMS, et al. Hypoxia Converts Human Macrophages Into Triglyceride-Loaded Foam Cells. Arterioscler Thromb Vasc Biol 2006; 26(8): 1871-1876.

132. Tian L, Luo N, Klein RL, Chung BH, Garvey WT, Fu Y. Adiponectin reduces lipid accumulation in macrophage foam cells. Atherosclerosis 2009; 202(1): 152-161.

133. Volobueva A, Zhang D, Grechko AV, Orekhov AN. Foam cell formation and cholesterol trafficking and metabolism disturbances in atherosclerosis. Cor et Vasa 2018.

134. Ouimet M, Ediriweera H, Afonso MS, Ramkhelawon B, Singaravelu R, Liao X, et al. microRNA-33 Regulates Macrophage Autophagy in Atherosclerosis. Arterioscler Thromb Vasc Biol 2017; 37(6): 1058-1067.

135. Wang M, Wu H, Fu G, Zhang H, Zhou X, Tang L, et al. Acetyl-coenzyme A carboxylase alpha promotion of glucose-mediated fatty acid synthesis enhances survival of hepatocellular carcinoma in mice and patients. Hepatology 2016; 63(4): 1272-1286.

136. Rosenblat M, Coleman R, Reddy ST, Aviram M. Paraoxonase 2 attenuates macrophage triglyceride accumulation via inhibition of diacylglycerol acyltransferase 1. J Lipid Res 2009; 50(5): 870-879.

137. Rigamonti E, Helin L, Lestavel S, Mutka AL, Lepore M, Fontaine C, et al. Liver X Receptor Activation Controls Intracellular Cholesterol Trafficking and Esterification in Human Macrophages. Circ Res 2005; 97(7): 682-689.

138. Ringseis R, Wen G, Saal D, Eder K. Conjugated Linoleic Acid Isomers Reduce Cholesterol Accumulation in Acetylated LDL-Induced Mouse RAW264.7 Macrophage-Derived Foam Cells. Lipids 2008; 43(10): 913-923.

139. Linton MF, Hasty AH, Babaev VR, Fazio S. Hepatic apo E expression is required for remnant lipoprotein clearance in the absence of the low density lipoprotein receptor. J Clin Invest 1998; 101(8): 1726-1736.

140. Schmidt V, Subkhangulova A, Willnow TE. Sorting receptor SORLA: Cellular mechanisms and implications for disease. Cellular and Molecular Life Sciences 2017; 74(8): 1475-1483.

141. Nilsson SK, Christensen S, Raarup MK, Ryan RO, Nielsen MS, Olivecrona G. Endocytosis of Apolipoprotein A-V by Members of the Low Density Lipoprotein Receptor and the Vps10p Domain Receptor Families. Journal of Biological Chemistry 2008; 283(38): 25920-25927.

142. Klinger SC, Glerup S, Raarup MK, Mari MC, Nyegaard M, Koster G, et al. SorLA regulates the activity of lipoprotein lipase by intracellular trafficking. J Cell Sci 2011; 124(7): 1095-1105.

143. Babaev VR, Fazio S, Gleaves LA, Carter KJ, Semenkovich CF, Linton MF. Macrophage lipoprotein lipase promotes foam cell formation and atherosclerosis in vivo. J Clin Invest 1999; 103(12): 1697-1705.

144. Aung HH, Lame MW, Gohil K, An CI, Wilson DW, Rutledge JC. Induction of ATF3 Gene Network by Triglyceride-Rich Lipoprotein Lipolysis Products Increases Vascular Apoptosis and Inflammation. Arterioscler Thromb Vasc Biol 2013; 33(9): 2088-2096.

145. Wang YI, Bettaieb A, Sun C, DeVerse JS, Radecke CE, Mathew S, et al. Triglyceride-rich lipoprotein modulates endothelial vascular cell adhesion molecule (VCAM)-1 expression via differential regulation of endoplasmic reticulum stress. PLoS One 2013; 8(10): e78322.

146. da Silva MK, de Carvalho ACG, Alves EHP, da Silva FRP, Pessoa LDS, Vasconcelos DFP. Genetic factors and the Risk of Periodontitis Development: Findings from a Systematic Review Composed of 13 Studies of Meta-Analysis with 71,531 Participants. International Journal of Dentistry 2017; 2017: 1914073.

147. RoadMap Epigenomics Project. RoadMap Epigenomics Project: Standards and Guidelines for Whole Genome Shotgun Bisulfite Sequencing . 2011; Available from: http://twww.roadmapepigenomics.org/files/protocols/data/dna-methylation/MethylC-SeqStandards_FINAL.pdf. [cited June 9,2020].

148. Kim M, Long TI, Arakawa K, Wang R, Yu MC, Laird PW. DNA Methylation as a Biomarker for Cardiovascular Disease Risk. PLoS One 2010; 5(3): e9692.

149. Stenvinkel P, Karimi M, Johansson S, Axelsson J, Suliman M, Lindholm B, et al. Impact of inflammation on epigenetic DNA methylation - a novel risk factor for cardiovascular disease? J Intern Med 2007; 261(5): 488-499.

150. Zaina S, Heyn H, Carmona FJ, Varol N, Sayols S, Condom E, et al. DNA Methylation Map of Human Atherosclerosis. Circ Cardiovasc Genet 2014; 7(5): 692-700.

151. Wang Z, Li X, Jiang Y, Shao Q, Liu Q, Chen B, et al. swDMR: A Sliding Window Approach to Identify Differentially Methylated Regions Based on Whole Genome Bisulfite Sequencing. PLoS One 2015; 10(7): e0132866.

152. Xu J, Zhou S, Gong X, Song Y, van Nocker S, Ma F, et al. Single-base methylome analysis reveals dynamic epigenomic differences associated with water deficit in apple. Plant Biotechnol J 2018; 16(2): 672-687.

153. Chan LC, Rossetti M, Miller LS, Filler SG, Johnson CW, Lee HK, et al. Protective immunity in recurrent *Staphylococcus aureus* infection reflects localized immune signatures and macrophage-conferred memory. Proc Natl Acad Sci USA 2018; 115(47): E11111-E11119.

154. Quintin J, Saeed S, Martens JA, Giamarellos-Bourboulis EJ, Ifrim DC, Logie C, et al. *Candida albicans* Infection Affords Protection against Reinfection via Functional Reprogramming of Monocytes. Cell Host & Microbe 2012; 12(2): 223-232.

155. Santecchia I, Vernel-Pauillac F, Rasid O, Quintin J, Gomes-Solecki M, Boneca IG, et al. Innate immune memory through TLR2 and NOD2 contributes to the control of *Leptospira interrogans* infection. PLOS Pathogens 2019; 15(5): e1007811.

156. Karunakaran D, Thrush AB, Nguyen M, Richards L, Geoffrion M, Singaravelu R, et al. Macrophage Mitochondrial Energy Status Regulates Cholesterol Efflux and is Enhanced by Anti-miR33 in Atherosclerosis. Circ Res 2015; 117(3): 266-278.

157. Aronis A, Madar Z, Tirosh O. Mechanism underlying oxidative stress-mediated lipotoxicity: Exposure of J774.2 macrophages to triacylglycerols facilitates mitochondrial reactive oxygen species production and cellular necrosis. Free Radical Biology and Medicine 2005; 38(9): 1221-1230.

158. Peng W, Cai G, Xia Y, Chen J, Wu P, Wang Z, et al. Mitochondrial Dysfunction in Atherosclerosis. DNA Cell Biol 2019; 38(7): 597-606.

159. Weiss-Sadan T, Maimoun D, Oelschlagel D, Kaschani F, Misiak D, Gaikwad H, et al. Cathepsins Drive Anti-Inflammatory Activity by Regulating Autophagy and Mitochondrial Dynamics in Macrophage Foam Cells. Cell Physiol and Biochem 2019; 53(3): 550-572.

160. Amézaga N, Sanjurjo L, Julve J, Aran G, Pérez-Cabezas B, Bastos-Amador P, et al. Human scavenger protein AIM increases foam cell formation and CD36-mediated oxLDL uptake. J Leukoc Biol 2014; 95(3): 509-520.

161. Yang Y, Li X, Peng L, An L, Sun N, Hu X, et al. Tanshindiol C inhibits oxidized low-density lipoprotein induced macrophage foam cell formation via a peroxiredoxin 1 dependent pathway. Biochim Biophys Acta Mol Basis Dis 2018; 1864(3): 882-890.

162. Morawietz H, Duerrschmidt N, Niemann B, Galle J, Sawamura T, Holtz J. Augmented endothelial uptake of oxidized low-density lipoprotein in response to endothelin-1. Clin Sci (Lond) 2002; 103(suppl_48): 9S-12S.

163. Chen JW, Zhou SB, Tan ZM. Aspirin and pravastatin reduce lectin-like oxidized low density lipoprotein receptor-1 expression, adhesion molecules and oxidative stress in human coronary artery endothelial cells. Chin Med J (Engl) 2010; 123(12): 1553-1556.

164. Zmijewski JW, Moellering DR, Le Goffe C, Landar A, Ramachandran A, Darley-Usmar VM. Oxidized LDL induces mitochondrially associated reactive oxygen/nitrogen species formation in endothelial cells. Am J Physiol Heart Circ Physiol 2005; 289(2): H852-H861.

165. Zhang C, Adamos C, Oh MJ, Baruah J, Ayee MAA, Mehta D, et al. oxLDL induces endothelial cell proliferation via Rho/ROCK/Akt/p27kip1 signaling: opposite effects of oxLDL and cholesterol loading. Am J Physiol Cell Physiol 2017; 313(3): C340-C351.

166. Linsel-Nitschke P, Jansen H, Aherrarhou Z, Belz S, Mayer B, Lieb W, et al. Macrophage cholesterol efflux correlates with lipoprotein subclass distribution and risk of obstructive

coronary artery disease in patients undergoing coronary angiography. Lipids Health Dis 2009; 8:14.

167. Bonacina F, Coe D, Wang G, Longhi MP, Baragetti A, Moregola A, et al. Myeloid apolipoprotein E controls dendritic cell antigen presentation and T cell activation. Nature Communications 2018; 9(1): 3083.

168. Ramond E, Jamet A, Coureuil M, Charbit A. Pivotal Role of Mitochondria in Macrophage Response to Bacterial Pathogens. Frontiers in Immunology 2019; 10: 2461.

169. van Tits LJH, Stienstra R, van Lent PL, Netea MG, Joosten LAB, Stalenhoef AFH. Oxidized LDL enhances pro-inflammatory responses of alternatively activated M2 macrophages: A crucial role for Krüppel-like factor 2. Atherosclerosis 2011; 214(2): 345-349.

170. Wei X, Song H, Yin L, Rizzo MG, Sidhu R, Covey DF, et al. Fatty acid synthesis configures the plasma membrane for inflammation in diabetes. Nature 2016; 539(7628): 294-298.

171. Brand K, Mackman N, Curtiss LK. Interferon-gamma Inhibits Macrophage Apolipoprotein E Production by Posttranslational Mechanisms. J Clin Invest 1993; 91(5): 2031-2039.

172. Yu S, Ding L, Liang D, Luo L. *Porphyromonas gingivalis* inhibits M2 activation of macrophages by suppressing α-ketoglutarate production in mice. Mol Oral Microbiol 2018; 33(5): 388-395.

173. Lam RS, O'Brien-Simpson NM, Lenzo JC, Holden JA, Brammar GC, Walsh KA, et al. Macrophage Depletion Abates *Porphyromonas gingivalis*-Induced Alveolar Bone Resorption in Mice. J Immunol 2014; 193(5): 2349-2362.

174. Zhuang Z, Yoshizawa-Smith S, Glowacki A, Maltos K, Pacheco C, Shehabeldin M, et al. Induction of M2 Macrophages Prevents Bone Loss in Murine Periodontitis Models. J Dent Res 2019; 98(2): 200-208.

175. Smith JD. New Role of Histone Deacetylase 9 in Atherosclerosis and Inflammation. Arterioscler Thromb Vasc Biol 201; 34(9): 198-1799.

176. Harman JL, Dobnikar L, Chappell J, Stokell BG, Dalby A, Foote K, et al. Epigenetic Regulation of Vascular Smooth Muscle Cells by Histone H3 Lysine 9 Dimethylation Attenuates Target Gene-Induction by Inflammatory Signalling. Arterioscler Thromb Vasc Biol 2019; 39(11): 2289-2302.

177. Akalin FA, Baltacioğlu E, Alver A, Karabulut E. Lipid peroxidation levels and total oxidant status in serum, saliva and gingival crevicular fluid in patients with chronic periodontitis. J Clin Periodontol 2007; 34(7): 558-565.

178. Ambati M, Rani KR, Reddy PV, Suryaprasanna J, Dasari R, Gireddy H. Evaluation of oxidative stress in chronic periodontitis patients following systemic antioxidant supplementation: A clinical and biochemical study. J Nat Sci Biol Med 2017; 8(1): 99-103.

179. Liu Z, Liu Y, Song Y, Zhang X, Wang S, Wang Z. Systemic Oxidative Stress Biomarkers in Chronic Periodontitis: A Meta-Analysis. Dis Markers 2014; 2014: 931083.

180. Maghbooli Z, Hossein-nezhad A, Larijani B, Amini M, Keshtkar A. Global DNA methylation as a possible biomarker for diabetic retinopathy. Diabetes Metab Res Rev 2015 Feb;31(2):183-189.

181. Yan J, Tie G, Wang S, Tutto A, DeMarco N, Khair L, et al. Diabetes impairs wound healing by Dnmt1-dependent dysregulation of hematopoietic stem cells differentiation towards macrophages. Nature Communications 2018; 9(1): 33.

182. Liu W, Cao Y, Dong L, Zhu Y, Wu Y, Lv Z, et al. Periodontal therapy for primary or secondary prevention of cardiovascular disease in people with periodontitis. Cochrane Database Syst Rev 2019;12(12): CD009197.

183. Merchant A. Periodontal Health and Cardiovascular Disease Risk: Association or Causation? 2016; Available from: https://www.acc.org/latest-in-cardiology/articles/2016/08/15/13/38/periodontal-health-and-cardiovascular-disease-risk. [cited June 10, 2020].

184. Duncan MS, Freiberg MS, Greevy RA,Jr, Kundu S, Vasan RS, Tindle HA. Association of Smoking Cessation with Subsequent Risk of Cardiovascular Disease. JAMA 2019; 322(7): 642-650.

185. Cholesterol Treatment Trialists' (CTT) Collaborators, Mihaylova B, Emberson J, Blackwell L, Keech A, Simes J, et al. The effects of lowering LDL cholesterol with statin therapy in people at low risk of vascular disease: Meta-analysis of individual data from 27 randomised trials. Lancet 2012; 380(9841): 581-590.

186. Gallagher KA, Joshi A, Carson WF, Schaller M, Allen R, Mukerjee S, et al. Epigenetic Changes in Bone Marrow Progenitor Cells Influence the Inflammatory Phenotype and Alter Wound Healing in Type 2 Diabetes. Diabetes 2015; 64(4): 1420-1430.

187. Li Y, Seto E. HDACs and HDAC Inhibitors in Cancer Development and Therapy. Cold Spring Harbor Perspectives in Medicine 2016; 6(10): a026831.

188. Gonzalez-Fierro A, Dueñas-González A. Emerging DNA methylation inhibitors for cancer therapy: challenges and prospects. Expert Review of Precision Medicine and Drug Development 2019; 4(1): 27-35.